

# UNDERWATER ACOUSTIC MODEM USING OFDM

A THESIS

SUBMITTED TO THE DEPARTMENT OF ELECTRICAL AND

ELECTRONICS ENGINEERING

AND THE GRADUATE SCHOOL OF ENGINEERING AND SCIENCES

OF BILKENT UNIVERSITY

IN PARTIAL FULFILLMENT OF THE REQUIREMENTS

FOR THE DEGREE OF

MASTER OF SCIENCE

By

Mine Merve Yüksel

January 2012

I certify that I have read this thesis and that in my opinion it is fully adequate,  
in scope and in quality, as a thesis for the degree of Master of Science.

---

Prof. Dr. Hayrettin Köyメン (Supervisor)

I certify that I have read this thesis and that in my opinion it is fully adequate,  
in scope and in quality, as a thesis for the degree of Master of Science.

---

Assist. Prof. Dr. Sinan Gezici

I certify that I have read this thesis and that in my opinion it is fully adequate,  
in scope and in quality, as a thesis for the degree of Master of Science.

---

Assist. Prof. Dr. Arif Sanlı Ergün

Approved for the Graduate School of Engineering and Sciences:

---

Prof. Dr. Levent Onural  
Director of Graduate School of Engineering and Sciences

# ABSTRACT

## UNDERWATER ACOUSTIC MODEM USING OFDM

**Mine Merve Yüksel**

**M.S. in Electrical and Electronics Engineering**

**Supervisor: Prof. Dr. Hayrettin Köyメン**

**January 2012**

This thesis is about design, simulation and testing of an underwater acoustic modem using OFDM. The thesis work combines a theoretical part, whose objective is to understand the appropriate techniques to deal with the characteristics of the targeted channel, simulations and a practical part regarding the system deployment and experimental tests. There has been a great growing interest in transmitting real-time data and video. Unmanned underwater vehicles (UUVs) for military and scientific applications have become important. Building distributed and scalable underwater wireless sensor networks (UWSN) that will bring significant advantages and benefits to underwater applications, such as ocean observation for scientific exploration, commercial exploitation, coastline protection and target detection in military events has been in the scope of researchers. Based on these, designing a concrete system with high data rate will benefit many underwater acoustic (UWA) applications. The existing systems in literature use single carrier transmission and rely on linear or non-linear equalization techniques to suppress inter-symbol interference (ISI), however this requires complex equalizers and results in low data rates. Therefore we concentrate on multicarrier modulation. In this thesis ZP-OFDM (Zero Padded-Orthogonal Frequency Division Multiplexing) receiver is built, where CFO (Carrier Frequency Offset) compensation, pilot-tone based channel estimation, and data demodulation are carried out on the basis of each OFDM block. The implemented OFDM system has been developed in MATLAB. MATLAB scripts generate a data burst that contained OFDM blocks, and then they are

transmitted to the hardware from a laptop by using a Data Acquisition (DAQ) Card. At the other side of the system, the receiver laptop gets the data by using a DAQ Card. As the data is received, MATLAB scripts are demodulated and data is detected. Simulations aim to provide correct implementation of all the algorithms by coupling the generated OFDM signal to a channel using Bellhop underwater channel model and noise addition algorithm, that artificially introduces some of the real channel effects into the signal. The method is tested in a shallow-water experiment at Bilkent Lake. Over a bandwidth of 12 kHz, the data rate is 13.92 kb/s with QPSK modulation, when the number of subcarriers was 1024. Bit-error-rate (BER) is less than  $9 \times 10^{-2}$  without any coding.

*Keywords:* Multicarrier modulation, orthogonal frequency division multiplexing (OFDM), underwater acoustic (UWA) communication.

# ÖZET

## OFDM KULLANAN SUALTI AKUSTİK MODEM

Mine Merve Yüksel

Elektrik ve Elektronik Mühendisliği Bölümü Yüksek Lisans

Tez Yöneticisi: Prof. Dr. Hayrettin Köyメン

Ocak 2012

Bu tezde dikey frekans bölmeli çöklama (OFDM) kullanan bir sualtı akustik modemin tasarımı, simülasyonu ve testi anlatılmıştır. Tez, hedeflenen kanalın özelliklerine uygun teknikleri anlatan teorik kısmı, simülasyonları ve sistem kurulumu ve testleri anlatan pratik kısmı birleştirir. Gerçek zamanlı veri ve video göndermeye ilgi artmıştır. Askeri ve bilimsel uygulamalar için insansız sualtı araçları(UUVs) önemli hale gelmiştir. Sualtı uygulamalarına önemli faydalı getirecek bilimsel keşifler için okyanus gözlemi, ticari araştırmalar, kıyı şeridi koruma ve hedef tespiti kapsamında dağıtık ve ölçeklenebilir kablosuz sualtı sensör ağları (UWSN) geliştirmek araştırmacıların hedefindedir. Buna dayanarak, yüksek veri hızı olan somut bir sistem tasarımindan birçok sualtı akustik uygulamasında yararlanılacaktır. Literatürde mevcut sistemler , tek taşıyıcılı iletişim ve semboller arası girişimi( ISI) bastırmak amacıyla doğrusal veya doğrusal olmayan denkleştirme teknikleri kullanmaktadır. Bu karmaşık denkleştiriciler gerektirir ve düşük veri aktarım hızına neden olur. Bu nedenle, çok taşıyıcılı modülasyon kullandık. Bu tezde, Sıfır ile Dolgulanmış -OFDM alıcısı geliştirilmiş ve taşıyıcı frekans ofseti, pilot-simbol destekli kanal kestirimini, ve veri demodülasyonu her OFDM blok bazında yapılmıştır. OFDM sistemi MATLAB ortamında geliştirilmiştir. MATLAB kodları tarafından oluşturulan ve OFDM blokları içeren veri paketleri kullanılan veri edinme (DAQ) kartı ile bir dizüstü bilgisayardan donanıma aktırılır. Sistemin diğer ucunda ise alıcı dizüstü bilgisayar bir veri edinme kartı sayesinde veriyi alır. Verinin alınması ile beraber, MATLAB kodları ile demodülasyon

işlemi gerçekleştirilir. Simülasyonlar, algoritmaların doğru uygulandığını görmek amacıyla, yaratılan OFDM sinyalini Bellhop sualtı kanal modeli ve gürültü kaynağından geçirerek yapılmıştır. Sistem, Bilkent Üniversitesi Gölet Tesisinde, sıç suda test edilmiştir. 12 kHz bant genişliği içinde, alttaşiyıcı sayısı 1024 iken dördün faz kaydırmalı modülasyonu(QPSK) ile veri aktarım hızı 13.92 kb/s olmuştur. Bit hata oranı (BER), herhangi bir kodlama olmadan  $9 \times 10^{-2}$ 'den daha azdır.

*Anahtar Kelimeler:* Çok Taşıyıcılı modülasyon, dikey frekans bölmeli çoklama (OFDM), sualtı akustik iletişim

# Acknowledgements

I would like to express my deepest respect and most sincere gratitude to my supervisor, Prof. Dr. Hayrettin Köymen, for his patient guidance and encouragement at all stages of my work. I have been extremely lucky to have a supervisor who cared so much about my work, and who responded to my questions and queries so promptly. I am also greatly indebted to his understanding in matters of non academic concern which have helped me endure some difficult times during my study period. I wish each student the honor and privilege to be his student.

I wish to thank the other member of my committee, Assist. Prof. Dr. Sinan Gezici of the Electrical and Electronics Department at Bilkent University. He has always willingly supported me since my undergraduate studies. He is always kind and he always helps his students. It was a great honor to be his student. I wish each student the opportunity to meet him and be his student.

I want to thank Assist. Prof. Dr. Arif Sanlı Ergün of Electrical and Electronics Department at TOBB University of Economy and Technology for accepting to evaluate my thesis and sit in the examination committee. His guidance was invaluable to this thesis. I also want to thank him for his support, help and kindness to my graduate studies.

I want to thank to Electrical and Electronics Department faculty and staff for all their dedication to their students.

I would like to thank my colleague Emrecan Demirörs for his help, discussions and comments in each part of my work. It was a great pleasure working with him.

I would like to thank my colleague Akif Sinan Taşdelen for his help in my research.

I would like to thank staff at Meteksan Defense Industry Inc. for their support during my thesis.

I would like to thank my parents Vildan and Levent Yüksel for their unending support and love.

# Table of Contents

	Page
Abstract . . . . .	iii
zett . . . . .	v
Acknowledgements . . . . .	vii
Table of Contents . . . . .	viii
List of Figures . . . . .	x
List of Tables . . . . .	xii
1 INTRODUCTION . . . . .	1
2 UNDERWATER ACOUSTIC COMMUNICATION CHANNEL . . . . .	4
2.1 Channel Characteristics . . . . .	6
2.1.1 Transmission Loss . . . . .	6
2.1.2 Noise . . . . .	8
2.1.3 Propagation Delay . . . . .	9
2.1.4 Doppler Effect . . . . .	9
2.2 Resource Allocation . . . . .	10
2.2.1 Signal to Noise Ratio . . . . .	10
2.2.2 Optimal Frequency . . . . .	11
2.2.3 Transmission Power . . . . .	11
3 ORTHOGONAL FREQUENCY DIVISION MULTIPLEXING . . . . .	15
3.1 General Description . . . . .	15
3.1.1 Mathematical Description . . . . .	16
3.1.2 Advantages and Drawbacks . . . . .	18
3.2 Intercarrier Interference . . . . .	19
3.2.1 Sources . . . . .	19
4 OFDM TRANSMITTER DESIGN . . . . .	22
4.1 System Model . . . . .	22
4.2 Implementation of Transmitter Algorithms . . . . .	24

4.2.1	IFFT Modulation . . . . .	24
4.2.2	Time Synchronization and Guard Time . . . . .	27
5	OFDM RECEIVER DESIGN . . . . .	28
5.1	System Model . . . . .	28
5.2	Receiver Algorithms . . . . .	29
5.2.1	Pilot Tone based Channel Estimation . . . . .	29
5.2.2	CFO Estimation . . . . .	31
6	EXPERIMENT SETTING . . . . .	33
6.1	Deployment . . . . .	33
6.2	Hardware . . . . .	33
7	RESULTS ON EXPERIMENTAL DATA . . . . .	37
7.1	Simulation Tests . . . . .	37
7.2	Underwater Experiment . . . . .	41
7.2.1	CFO and Channel Estimation . . . . .	44
7.2.2	BER Performance . . . . .	47
8	CONCLUSIONS . . . . .	51
	APPENDIX . . . . .	53
A	Datasheets . . . . .	53
B	Description of Bellhop Underwater Channel Model . . . . .	56

# List of Figures

2.1	Ocean as a cylindrical waveguide . . . . .	5
2.2	Acoustic Absorption as a function of temperature . . . . .	7
2.3	Multipath Effect . . . . .	12
2.4	ISI due to Multipath . . . . .	13
2.5	The typical sound levels of ocean background noises at different frequencies	14
3.1	Orthogonal overlapping spectral shapes for OFDM. . . . .	17
3.2	Frequency synchronization in OFDM systems . . . . .	20
3.3	Effect of the Doppler spread in the ICI phenomenon . . . . .	21
4.1	Transmitter System Model . . . . .	23
4.2	Packet Structure . . . . .	25
4.3	Transmitted Signal . . . . .	26
5.1	Receiver System Model . . . . .	28
6.1	Experimental Setup . . . . .	33
6.2	Bilkent Lake Facility . . . . .	34
6.3	Transmission block diagram for underwater tests, transmitter(up) and receiver(bottom) . . . . .	36
7.1	Bellhop Ray Tracing . . . . .	38
7.2	System Model of the Simulator . . . . .	38
7.3	Simulation setup . . . . .	39
7.4	Received QPSK constellations of OFDM blocks . . . . .	40
7.5	Estimated Channel Response by suing PN sequence matching . . . . .	40
7.6	Ray paths which come from the shore reflection . . . . .	42
7.7	Received QPSK constellations of OFDM blocks . . . . .	43
7.8	BER for each OFDM block in a packet . . . . .	43
7.9	Estimated Channel Response by suing PN sequence matching . . . . .	44

7.10 Received Signal . . . . .	45
7.11 CFO Estimation . . . . .	46
7.12 Channel Estimation for all blocks . . . . .	47
7.13 Scatter plot for received QPSK signals . . . . .	48
7.14 BER for each OFDM block in a packet . . . . .	48
7.15 Estimated Channel response by using PN sequence matching . . . . .	50
A.1 Power response of the Krohn-Hite Model 7500 Power Amplifier . . . . .	54
A.2 Horizontal directivity pattern (left) and receiving sensitivity (right) of the Reson TC4040 hydrophone . . . . .	55
A.3 High-pass filter (left) and low-pass filter (right) frequency responses of the Reson VP2000 preamplifier . . . . .	55

# List of Tables

7.1 System Parameters of ZP-OFDM block . . . . .	41
--	----

# Chapter 1

## INTRODUCTION

Two-thirds of the surface of the Earth is covered by water. Humans are curious about unexplored world of underwater. Recently, there has been a growing interest in monitoring underwater for scientific exploration, commercial exploitation, and to protect from attack. There has been a great growing interest in transmitting real-time data, video and sonar images. Unmanned underwater vehicles (UUVs) for military and scientific applications has become important[1]. Building distributed and scalable underwater wireless sensor networks (UWSN) that will bring significant advantages and benefits to underwater applications, such as ocean observation for scientific exploration, commercial exploitation, coastline protection and target detection in military events [2], [3] has been in the scope of researchers. Establishing effective underwater acoustic (UWA) communications will help the development of UWSNs.

The unique characteristics of underwater acoustic channel pose great challenges to communications. Since electromagnetic waves do not propagate well in underwater environments, underwater communications have to rely on other physical means, such as sound, to transmit signals. Due to the reverberation effect where the receiver observes multipath signals bounced from the surface and the bottom, underwater acoustic channels usually have large delay spread, leading to strong frequency selectivity. On the other hand, UWA channels exhibit high time-variation temporally and spatially. Being both frequency and time selective, UWA channel poses great challenges for high performance and high rate communications.

Existing coherent underwater communication uses single carrier transmission and relies on linear or non-linear equalization techniques to suppress inter-symbol interference (ISI) [4]. The canonical receiver in [5], which demonstrates the feasibility of phase coherent modulation, relies on an adaptive decision feedback equalizer coupled with delay and phase

tracking. As the data rate increases, the symbol duration decreases, and thus a channel with the same delay spread contains more channel taps when converted to the baseband discrete-time model. This imposes great challenges for the channel equalizer, whose complexity will prevent rate improvement with the existing single-carrier approach.

Multicarrier modulation in the form of orthogonal frequency division multiplexing (OFDM) has been quite successful in broadband wireless communication over radio channels, e.g., wireless local area networks (IEEE 802.11a/g/n) [6], and wireless metropolitan area networks (IEEE 802.16) [7], [8]. OFDM divides the available bandwidth into a large number of overlapping subbands, so that the symbol duration is long compared to the multipath spread of the channel. Consequently, ISI may be neglected in each subband, that greatly simplifies the receiver complexity on channel equalization. This success motivates researchers to work on OFDM in underwater acoustic communications.

The existing literature focused mostly on conceptual system analysis and simulation based studies [9], [10] , [11], [12] until Prof. Milica Stojanovic and her co-researchers provided successful experimental results [13] ,[14], [15]. This thesis is based on the work and algorithms of Prof. Milica Stojanovic and her co-researchers [13] ,[14], [15]. Our system is adapted from their work.

This thesis describes the design, simulation and testing of a pilot-tone based ZP-OFDM (Zero Padded-Orthogonal Frequency Division Multiplexing) receiver, where CFO (Carrier Frequency Offset) compensation, channel estimation, and data demodulation are carried out on the basis of each OFDM block. We use ZP-OFDM modulation instead of cyclic prefix(CP). The reason behind is that CP can spend too much transmission power and it is not so effective in underwater channels where long delay spread occurs [16]. In the transmitter model, rectangular pulse shaping is used with IFFT modulation. QPSK modulation is done. CFO estimation is performed by least squares (LS) fitting error.

Simulations have been performed using Bellhop Underwater Acoustic Channel model [17] and aim to provide correct implementation of all the algorithms by coupling the generated OFDM signal to a channel simulation and noise addition algorithm, that artificially introduces some of the real channel effects into the signal. The method was tested in a shallow-water experiment at Bilkent Lake. Over a bandwidth of 12 kHz, the data rate is 13.92 kb/s with QPSK modulation, when the number of subcarriers is 1024. Bit-error-rate

(BER) is less than  $9 \times 10^{-2}$  without using any coding.

The rest of the thesis is organized as follows: Theoretical research is addressed between Chapters 2-6. In Chap. 2, underwater channel and its challenges are introduced. In Chap. 3, background on orthogonal frequency-division multiplexing (OFDM) is given. Chap. 4 includes transmitter design. In Chap. 5, receiver design is explained. Chap. 6 introduces the practical deployment for the experiments. The simulations are included as a part of the experimental work in Chap. 7, along with the information about the experiments. Finally, Chap. 8 concludes the analysis and gives some future work tips.

# **Chapter 2**

# **UNDERWATER ACOUSTIC COMMUNICATION CHANNEL**

Underwater acoustic (UWA) communication is a way of sending and receiving message below water. UWA channel is like a waveguide that is bounded by the sea floor and sea surface (See Fig. 2.1). There are several ways of employing such communication where the most common is using transducers. The state of the ocean environment directly affects underwater acoustic communication. For a successful establishment of an acoustic communication link under given environmental conditions, the physical communication channel must be taken into account.

Acoustic waves which result from variations of pressure in a medium are widely used as physical layer in UWA communications. Due to the greater density of water, they travel 4-5 times faster in water than they do in air (traveling in water at an average of 1500 m/s - the speed of sound subject to the water's temperature, salinity and pressure), but are about 5 orders of magnitude slower than electromagnetic waves. They have been widely used in underwater communication systems due to the relatively low attenuation of sound in water. Acoustic waves propagate at long distances through sea water only at extremely low frequencies (30-300 Hz). For lower distances higher frequencies may be used at the same time reducing the hardware requirements in terms of power and transducer characteristics. Underwater channel is one of the most demanding. There are several factors that impair signal reception in the ocean. Acoustic propagation is characterized by three major factors: attenuation that depends on the signal frequency, multipath propagation, and low speed of sound (1500 m/s). Variations in sound speed results in refraction of sound, which can weaken signal strength. The air-sea interface and the sea bottom boundary cause reflections, which generate severe multipath propagation that further distorts and disperses the

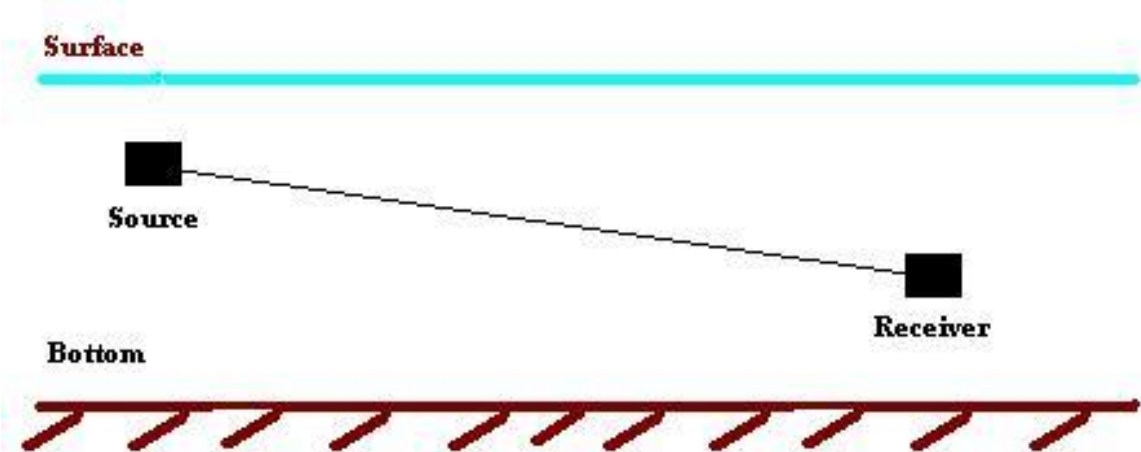


Figure 2.1: Ocean as a cylindrical waveguide

signal. Various noise sources in the ocean also deteriorate reception capability. Among these reasons, the major difficulties that adversely affect the acoustic waves are the following:

- Doppler is non-uniform across the signal bandwidth and more intensified than in radio channels,
- The communication bandwidth depends on the distance. As propagation is best supported at low frequencies, acoustic communication systems are inherently wideband,
- Attenuation is frequency-dependent,
- Due to the high attenuation and hardware constraints, received signals suffer from common low power which causes non negligible background noise,
- The speed of sound in underwater is around 1500 m/s and this results in large and variable propagation delays, high latency and relatively large motion-induced Doppler effects.

A summary of UWA channel and its major complications are discussed in this section.

## 2.1 Channel Characteristics

### 2.1.1 Transmission Loss

The transmission loss (TL) is defined as the decrease of the sound intensity through the path from the sender to the receiver. TL is usually expressed in terms of the logarithmic ratio of the sound intensity at a reference range of one meter away from the center of the acoustic source  $I_0$  and the sound intensity at the receiver  $I_1$  [18] :

$$TL = 10 \log\left(\frac{I_0}{I_1}\right) dB \quad (2.1)$$

For our interest, we can categorize absorption loss, spreading loss and multipath as main factors that add to total TL.

#### 2.1.1.1 Absorption Loss

The absorption loss is the TL due to viscous, thermal, and chemical relaxations. It depends on the temperature, salinity, and acidity of the sea water as well as the frequency of the sound wave. The formula for transmission loss due to absorption is:

$$TL_{absorption} = \alpha(r - 1) \quad dB \quad (2.2)$$

where  $\alpha$  is the absorption coefficient in dB/m and  $r$  is the range from the source in m. Other loss mechanisms such as scattering and bottom interactions can be included in the equation.

Diverse empirical expressions to measure the transmission loss have been developed. For seawater, the absorption coefficient at frequency  $f$  in kHz can be written as the sum of chemical relaxation processes and absorption from pure water [19] :

$$\alpha(f) = \frac{(A_1 P_1 f^2 f_1)}{(f^2 + f_1^2)} + \frac{(A_2 P_2 f^2 f_2)}{(f^2 + f_2^2)} + A_3 P_3 f^2 \quad (2.3)$$

where the first term is the contribution from boric acid with  $f_1$  as its relaxation frequency, the second term is from the contribution of magnesium sulphate with  $f_2$  and its relaxation frequency, and the third term is from the contribution of pure water. The pressure dependencies are given by  $P_1$ ,  $P_2$ , and  $P_3$  and  $A_1$ ,  $A_2$ , and  $A_3$  which are constants [20].

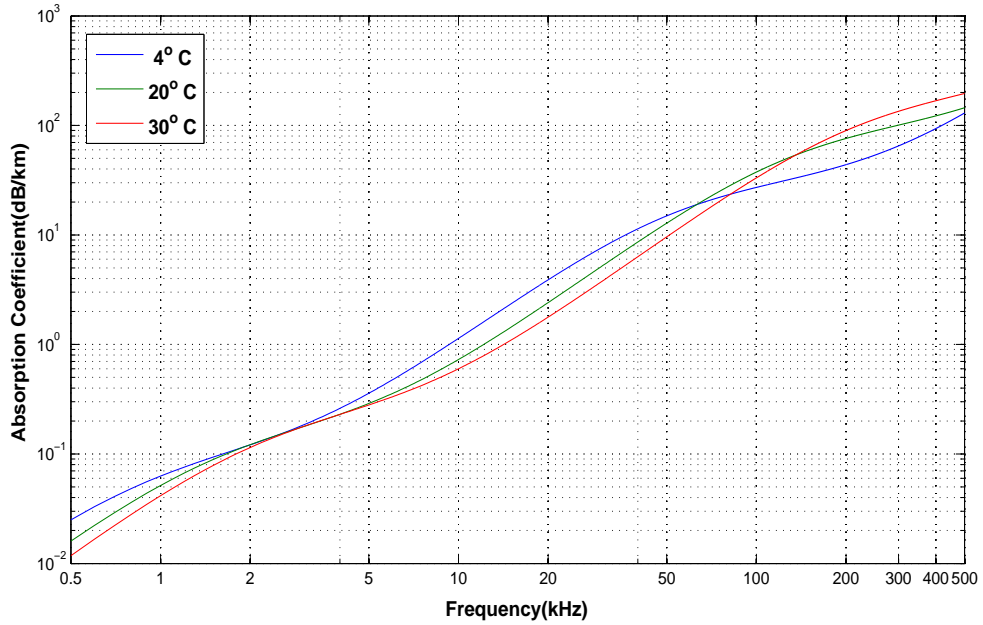


Figure 2.2: Acoustic Absorption as a function of temperature

There are many theoretical and empirical formulas to quantify the absorption coefficient  $\alpha$ . The absorption coefficient for frequencies above a few hundred Hz can be expressed empirically, using the Thorp's formula [21] :

$$\alpha(f) = \frac{0.11f^2}{f^2 + 1} + \frac{44f^2}{f^2 + 4100} + 2.75 \cdot 10^{-4}f^2 + 0.003 \quad \text{dB/km} \quad (2.4)$$

where  $f$  is in kHz.

Fig. 2.2 shows the variation in total absorption vs. frequency for different different temperatures. Since absorption coefficient increases with frequency, high frequency waves will be considerably attenuated within a short distance while low frequency acoustic waves can travel far. As a result, it puts a threshold to the maximal usable frequency.

### 2.1.1.2 Spreading Loss

As sound travels away from the source, acoustic energy spreads geometrically causing TL, which is called spreading loss. Spreading loss is frequency independent (when point sources/targets are used) while it depends on propagation range. In shallow water, sound is bounded by the surface and bottom resulting in cylindrical spreading. In deep water, the power loss caused by spreading is proportional to the square of the distance. In this

case, sound power loss increases linearly with the distance from the source. The formula for spreading loss is given in Eq. 2.5 :

$$TL_{spreading} = 10k \log(r) \quad \text{dB} \quad (2.5)$$

where  $k$  is spreading factor and  $r$  is range. For a practical underwater setting, the spreading loss falls somewhere between spherical and cylindrical spreading where  $k$  is between 1 (for cylindrical spreading) and 2 (for spherical spreading) [18] .

For our case, at Bilkent Lake where our experiments were done, although the water is bounded, transmission range is small so we accept spherical spreading.

### 2.1.1.3 Multipath

In underwater, there exist multiple paths from the transmitter to receiver, or multipath (See Fig. 2.3). Two fundamental mechanisms of multipath formation are reflection at the boundaries (bottom, surface and any objects in the water), and ray bending (as sound speed is a function of temperature, salinity, and depth, rays of sound always bend towards regions of lower propagation speed) [22]. Multipath can adversely affect communications because

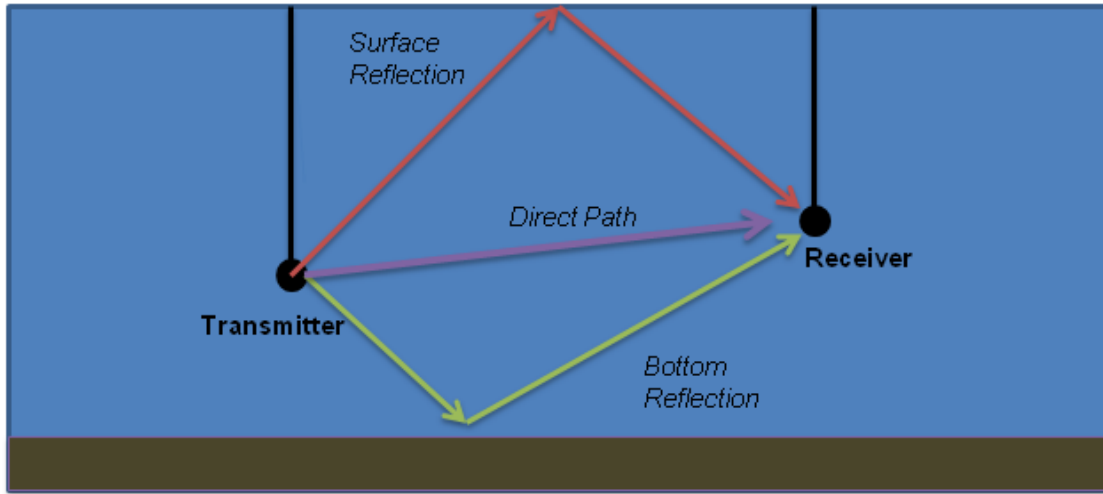


Figure 2.3: Multipath Effect

a large delay spread (the time difference of arrival of the first and last path at the receiver) introduces time dispersion of a signal, which causes severe inter-symbol interference (ISI) (See Fig. 2.4). Typical underwater channels may have a delay spread around 10ms, but

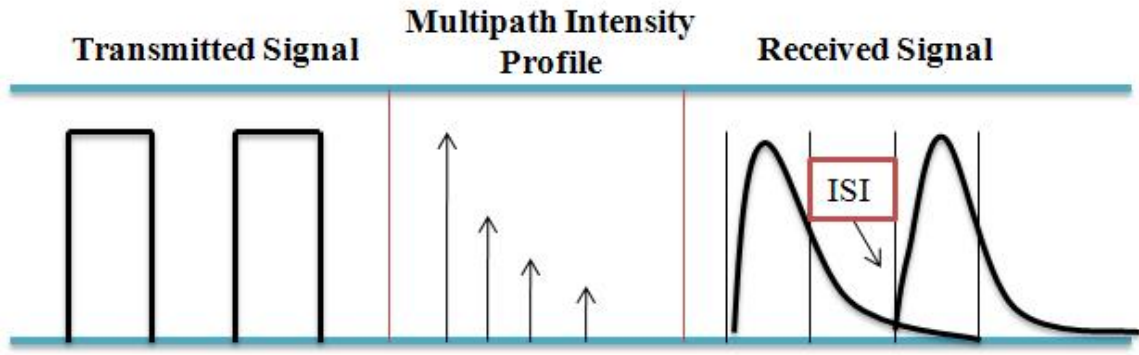


Figure 2.4: ISI due to Multipath

occasionally delay spread can be as large as 50 to 100ms [4] or as small as 3 ms [23]. Equalization should be done in the receiver in order to avoid distortions caused by multipath. In addition, ways to avoid ISI must be designed in order to correctly demodulate and detect the transmitted data. Later, in Chap. 5 a receiver algorithm for underwater acoustic channel that deals with multipath effects will be explained.

### 2.1.2 Noise

Ambient noise in the UWA channel originates from both natural and man-made sources. Naturally occurring noise is caused by biological and seismic activities and by hydrodynamic noise from waves, currents, tides, rain and wind. Man-made noise is mainly due to shipping activities. The primary source of ambient noise can be categorized by the frequency of sound. For frequencies below 10 Hz, turbulent noise dominates. In the frequency range of 10-200 Hz, ambient noise is primarily generated by distant shipping. In the range 200-100,000 Hz, ambient noise is mostly due to spray and bubbles associated with breaking waves, wind noise. At frequencies above 100 KHz, thermal noise (noise generated by the Brownian motion of water molecules) dominates [24].

Typical sound levels at different frequencies can be seen in Fig. 2.5 based on the formula by Coates [24]. The sound levels in this graph are dB relative to  $1 \mu\text{Pa}$ . When selecting a suitable frequency band for communication, besides path loss, noise should also be considered [26].

For our case, at Bilkent Lake where our experiments are done, transmission range is small

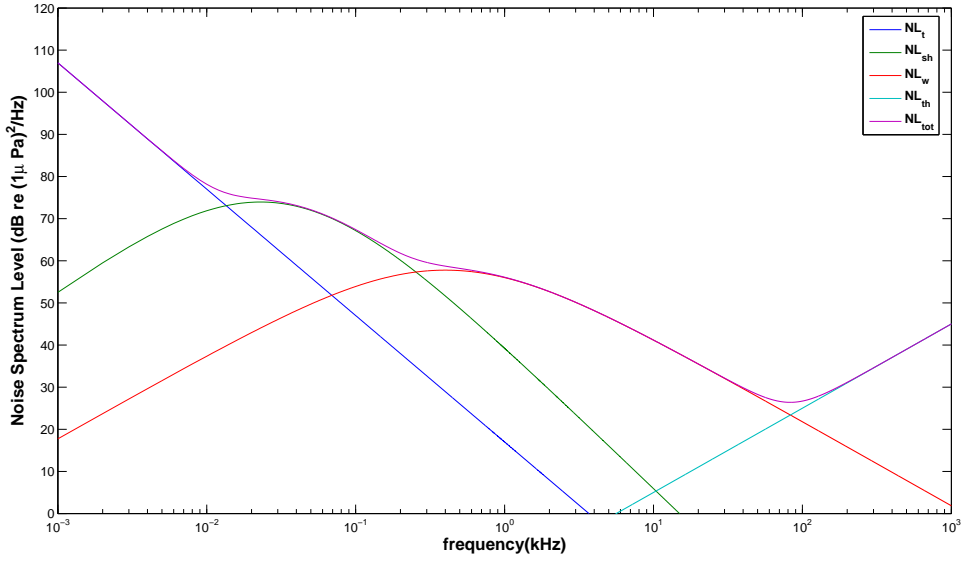


Figure 2.5: The typical sound levels of ocean background noises at different frequencies

and signal power is high so the environment is not noise limited. However, for other environments, effect of noise should be taken into account.

### 2.1.3 Propagation Delay

The nominal speed of sound in water is 1,500 m/s, when compared to the speed of electromagnetic waves in open-air, there is a difference on the orders magnitude. One of the main problems that results from low speed of sound is large propagation delays and high latency. This becomes a major complication for the application of feedback to correct the channel distortions.

### 2.1.4 Doppler Effect

In UWA communications, carrier tracking and symbol synchronization are adversely affected by Doppler. The low velocity of acoustic waves and the use of wideband modulation result in Doppler shifts that are several orders of magnitude greater than those experienced in EM transmission. Relative motion of the transmitting and receiving elements is usually unavoidable, particularly if either end of the link is deployed by a surface vessel which is subject to the effects of sea currents and/or surface waves. Rapidly moving platforms such

as autonomous underwater vehicles (AUVs) present a more serious problem. The non negligible Doppler causes a shift in the frequency components of the transmitted signal. The relative Doppler shift ( $\Delta$ ) is defined as the ratio of the source relative velocity ( $v$ ) to the propagation wave velocity ( $c$ ). For a single-frequency component  $w_n$ , the Doppler effect can be expressed as a frequency scaling,

$$\omega_{n^*} = \omega_n(1 + \Delta) \quad (2.6)$$

In underwater environments  $c$  is much lower than in open-air, so the Doppler effect is not ignorable. In addition, the fact that underwater systems are wideband causes much different Doppler shifts for different frequency components of the transmitted signal. This is typically known as frequency spreading. It is of key importance that underwater acoustic systems deal with non-uniform Doppler effect. As an example, a bad correction in a multicarrier system could cause Inter-Carrier Interference (ICI), which happens when some distortion due to other subcarriers' information is present in a selected channel.

## 2.2 Resource Allocation

Considering the adverse underwater environmental conditions such as propagation loss and ambient noise as well as some system constraints, one can determine the optimal frequency allocation for communication signals. The possibilities in terms of usable frequency bands are not numerous, due to acoustic path propagation and noise characteristics.

### 2.2.1 Signal to Noise Ratio

If we define a narrow band of frequencies of width  $\Delta f$  around some frequency  $f$ , the signal-to-noise ratio (SNR) in this band can be expressed as:

$$SNR(l, f) = \frac{S_l(f)}{A(l, f)N(f)} \quad (2.7)$$

where  $l$  is distance to the receiver and  $S_l(f)$  is the power spectral density of the transmitted signal, whose power may be adjusted according to the distance. For any given distance, the narrow-band SNR is thus a function of frequency. From this formula it becomes obvious that the acoustic bandwidth depends on the transmission distance. The bandwidth is

severely limited at longer distances. At shorter distances, the bandwidth increases, but it will ultimately be limited by that of the transducer.

Another important observation to be made is that the acoustic bandwidth is centered at low frequencies. In fact, the acoustic bandwidth  $B$  is often on the order of its center frequency  $f_c$ , which makes an acoustic communication system inherently wideband. This fact in turn bears significant implications on the design of signal processing methods, as it prevents one from making the narrowband assumption ( $B \ll f_c$ ), on which many radio communication principles are based [22] .

### 2.2.2 Optimal Frequency

For each distance  $l$  there clearly exists an optimal frequency  $f_o(l)$  for which the maximal narrow-band SNR is obtained at the receiver.

Ideally, when implementing a communication system, some transmission bandwidth around  $f_o(l)$  is chosen. The transmission power is adjusted so as to achieve the desired SNR level throughout the selected frequency band.

### 2.2.3 Transmission Power

Once the transmission bandwidth is set, the transmission power  $P(l)$  can be adjusted to achieve a desired narrowband SNR level corresponding to the 3 dB bandwidth  $B_{3dB}(l)$ . If we denote by  $S_l(f)$  the power spectral density (p.s.d) of the transmitted signal chosen for the distance  $l$ , then the total transmitted power is:

$$P(l) = \int_{B_{3dB}(l)} S_l(f) df = SNR_0 B_{3dB}(l) \frac{\int_{B_{3dB}(l)} N(f) df}{\int_{B_{3dB}(l)} A^{-1}(l, f) df} \quad (2.8)$$

where the transmitted signal p.s.d. is considered constant in the signal bandwidth.

# Chapter 3

## ORTHOGONAL FREQUENCY DIVISION MULTIPLEXING

Orthogonal Frequency Division Multiplexing (OFDM) has gained a great deal of interest during the last few decades. It has been adopted for several broadband communication systems; such as digital video broadcasting, Asymmetric Digital Subscriber Line (ADSL) services, Wireless Local Area Networks (IEEE 802.11a/g/n), Worldwide Interoperability for Microwave Access (WiMAX) systems (IEEE 802.16e) and third generation cellular systems [27]. Success of OFDM in radio channels motivates its use in UWA channels.

### 3.1 General Description

Multicarrier modulation is an attractive alternative to single carrier broadband modulation on channels with frequency-selective distortion. It is based on the idea of dividing the total available bandwidth into many narrow subbands, such that the channel transfer function appears constant (ideal) within each subband. By doing so, the need for time-domain channel equalization is eliminated. Instead, the subbands have to be separated in the frequency domain, which is efficiently performed using only the Fast Fourier Transform (FFT). This efficient implementation using FFT can be executed for multicarrier modulation and detection when used with rectangular pulse shaping.

The modulation technique on which the project is based is the Orthogonal Frequency Division Multiplexing (OFDM). OFDM achieves an adequate transmitter/receiver complexity, appropriate capacity, and provides numerous possibilities for channel compensation. OFDM is a frequency-division multiplexing (FDM) scheme utilized as a digital multi-carrier modulation method. A large number of closely-spaced orthogonal subcarriers are used to carry data. Data is divided into several parallel data streams or channels, one for

each subcarrier. Each subcarrier is modulated with a conventional modulation scheme (QAM,PSK,..).

### 3.1.1 Mathematical Description

In this section a former description of the OFDM signals is shown. It is important to know that OFDM is formed by blocks each containing the transmission for the  $K$  subcarriers. Each block duration contains the effective symbol time and the guard interval

$$T = T' + T_g \quad (3.1)$$

where  $T_g$  stands for the guard time and it must be longer than channel impulse response length to prevent Inter-Symbol Interference (ISI) between two consecutive OFDM blocks.  $T'$  stands for the effective symbol duration and it is defined as  $T' = K/B$  where  $B$  is the overall system bandwidth and  $K$  is the number of subcarriers, the spacing between adjacent subcarriers is  $\Delta f = 1/T'$ . So, the subcarrier frequencies are:

$$f_k = f_0 + k\Delta f \quad k=0,\dots,K-1 \quad (3.2)$$

where  $f_0$  is the optional carrier frequency for a not baseband transmission. Each of the subcarriers contain a QAM symbol; typical modulations on the UWA channel are QPSK, 8PSK and low density QAM such as 16 or 32-QAM. It is assumed that all the subcarriers contain the same modulation level; unlike the Discrete Multitone Modulation (DMT) where each subcarrier varies the bandwidth efficiency depending on the SNR in that band.

From the OFDM definition we can derive an expression for the bandwidth efficiency, which is the ratio for the bit rate to the bandwidth

$$\frac{R}{B} = \frac{m\alpha}{1 + T_g B / K} \quad (3.3)$$

where  $m$  stands for the modulation level and its units are *bits = symbol* and for the case of QPSK is  $m = 2$  bits=symbol.  $\alpha$  is the coding efficiency, either for block or convolutional coding. In Eq. 3.3 it is clearly seen that the efficiency of the system increases as spacing between subcarriers  $B/K$  and the guard interval decrease. Each one of the mapped symbols is modulated with one subcarrier, that is if the symbol on the  $k$ -subcarrier is called  $d_k$  then

the baseband expression of the modulated signal for only one block is

$$b_s(t) = \sum_{k=0}^{K-1} d_k e^{j2\pi k \delta f t} \quad t=0, \dots T' \quad (3.4)$$

Equation 3.4 has the form of an IFFT operation. In fact, all the practical modulation schemes implement the OFDM modulation process as an IFFT due to its low-complexity and dedicated existing hardware. In the receiver side, an FFT will be key to retrieve the data. To transmit the signal, a guard interval must be added. This can be in the form of Cyclic Prefix (CP) or a simple Zero Padding (ZP) operation [16]. The first one is used in most of the radio systems for its capability to preserve the FFT/IFFT circularity converting a linear channel convolution into a circular without any additional processing and offering good synchronization via autocorrelation on the receiver. The latter is used when power saving is needed and it offers even better properties than CP, but additional computations should be done to the received signal.

The spectrum of a typical OFDM signal is like the one shown in Fig. 3.1.

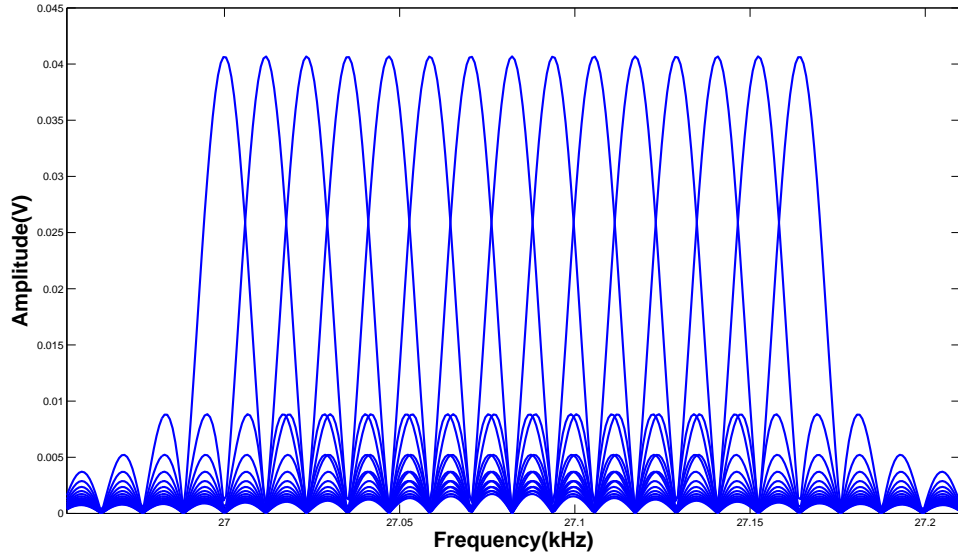


Figure 3.1: Orthogonal overlapping spectral shapes for OFDM.

The effective block symbol time is related to the subcarrier spacing to preserve the orthogonality between subcarriers. That is, for two specific subcarriers  $\phi_k(t)$ ,  $\phi_l(t)$  in the

demodulator

$$\int_0^{T'} \phi_k(t) \phi_l(t)^* = \int_0^{T'} e^{j2\pi k \delta f t} e^{-j2\pi l \delta f t} = \delta(k - l) \quad (3.5)$$

where  $\delta(t)$  is the Kronecker's delta. The orthogonality can be thought in time or in frequency domain. In time domain, as stated in previous equation, each subcarrier is a sine wave with an integer number of cycles within a block so, the definition of a scalar product of two sine waves with multiple frequencies is zero. From the frequency domain, the spectrum of each subcarrier is a *sinc* function with its maximum value in its center frequency while being zero at other subcarriers' centers.

### 3.1.2 Advantages and Drawbacks

In this section the main advantages and drawbacks of an OFDM system are given.

#### 3.1.2.1 Advantages

- Can easily adapt to severe channel conditions without complex equalization
- Robust against narrow-band co-channel interference
- Robust against Intersymbol interference (ISI) and fading caused by multipath propagation
- High spectral efficiency
- Efficient implementation using FFT
- Low sensitivity to time synchronization errors

#### 3.1.2.2 Drawbacks

- Sensitive to Doppler shift
- Sensitive to frequency synchronization problems
- High peak-to-average-power ratio (PAPR), requiring linear transmitter circuitry, which suffers from poor power efficiency.

- Loss of efficiency caused by Cyclic prefix/Guard interval.

Although there are some important factors in the drawbacks' list, OFDM is a good candidate to support high rate underwater communications.

## 3.2 Intercarrier Interference

One of the main causes of performance degradation is Intercarrier Interference (ICI). The main advantage of OFDM is that each subcarrier is orthogonal, and thus independent to each other. When the channel conditions change, orthogonality disappears and each subcarrier has some contribution to the others in the demodulating process. In this section, the sources of ICI are presented and a new OFDM signal model is also shown.

### 3.2.1 Sources

Although there may be many processes that can cause ICI, here we will focus on the ones that are more important in underwater communications.

#### 3.2.1.1 Doppler Shift

As shown in section 2.1.4, UWA channel suffers from severe Doppler effect due to the low carrier frequencies and the low speed of propagation of sound. The main cause of this effect is the relative motion between the ends of the transmission. As a further matter, the wideband nature of the signal impacts in two ways in its transformation. A frequency shift, and a time (de)compression. Recall from radio channels that time consequences are neglected in most of the cases and only frequency shift is considered. When talking about wireless OFDM in UWA communications it should be known that the Doppler shift can be sometimes comparable or even more than the subcarrier spacing. Conventionally, this shift is combated via resampling in time domain of the data, but its offset has to be known precisely. Produced ICI due to frequency de-synchronization is shown in Fig. 3.2. It can be seen that if correct synchronization is performed, no influence of any subcarrier is collected (although the example only shows two subcarriers for clarity, this can be extend to an arbitrary number). If the receiver oscillator has a little offset, or if there has been some

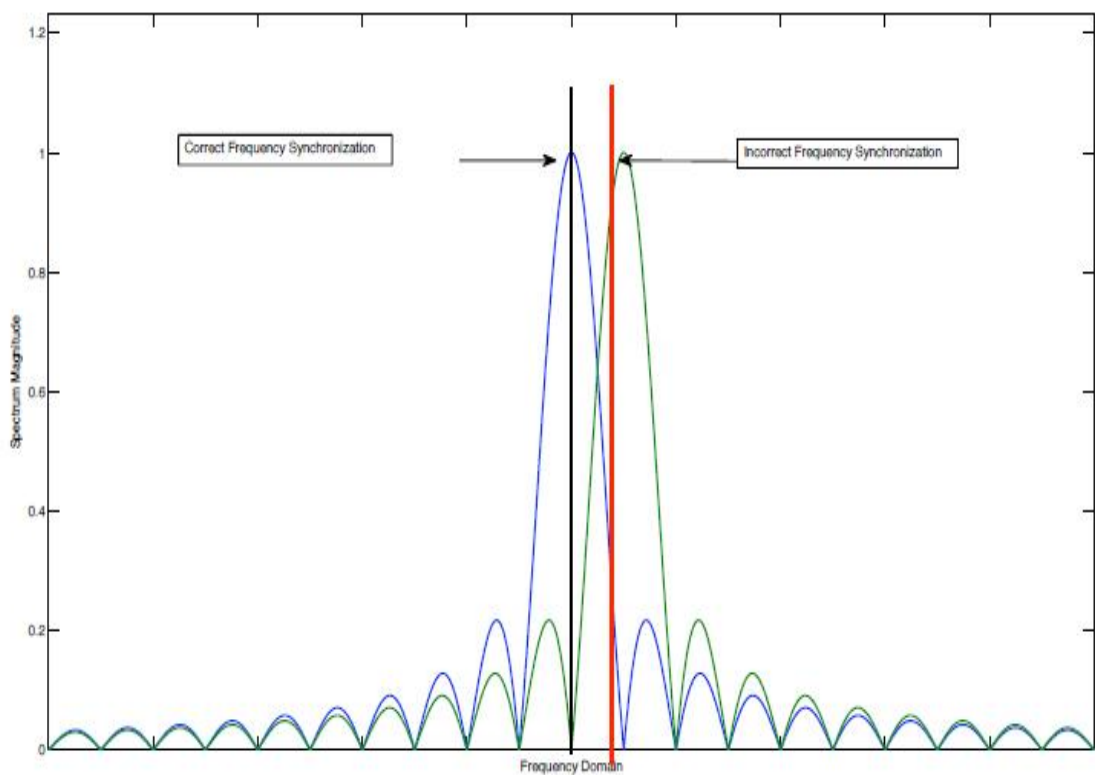


Figure 3.2: Frequency synchronization in OFDM systems

uncorrected Doppler shift, incorrect synchronization is then performed in the receiver and influence from other subcarriers are collected for one band as shown with the red line in the figure.

### 3.2.1.2 Channel Time-Variance and Doppler Spread

In OFDM, the channel is supposed to be time invariant within a block. If this condition is not satisfied, again, the subcarriers loose their orthogonality. Intuitively, Fig. 3.3 shows

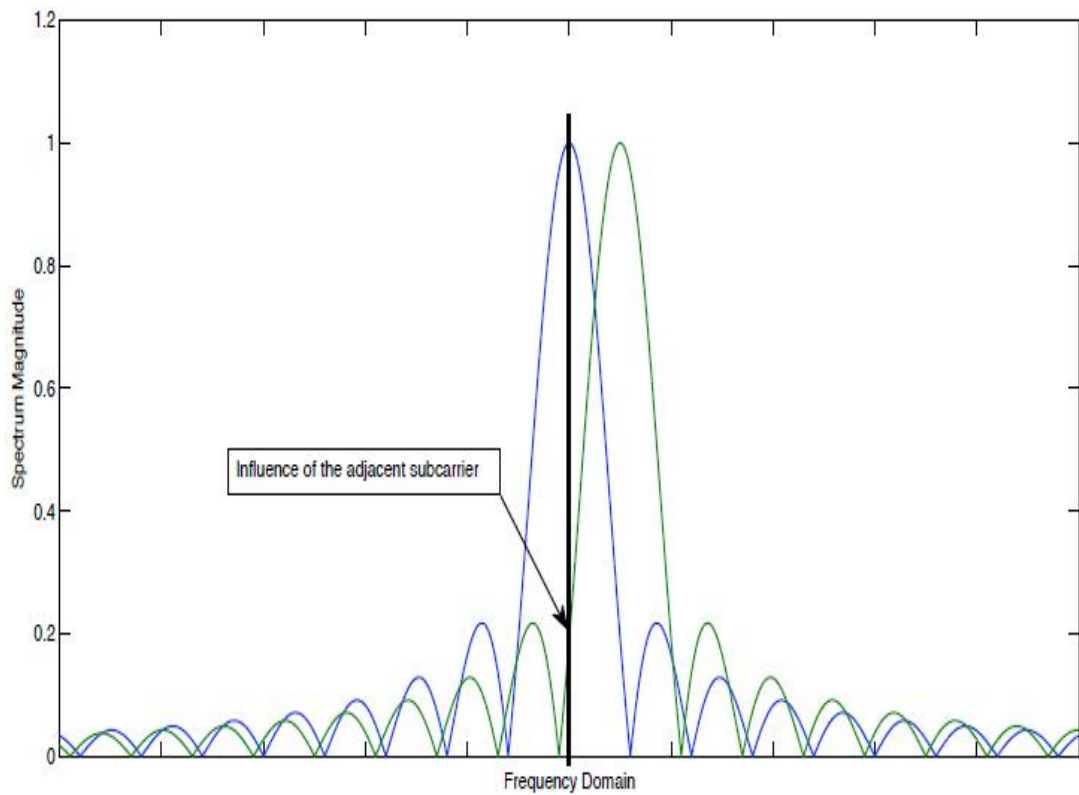


Figure 3.3: Effect of the Doppler spread in the ICI phenomenon

how this effect can lead to a degradation of the performance. Coherence time of the UWA channel is a critic parameter. Unlike radio communications, the lack of high bandwidths can make a transmission of an OFDM block with a high number of subcarriers last for a few milliseconds. In this time, the channel can change noticeably and time invariability is no longer respected. Those system will suffer of severe ICI, if nothing is done about it.

# Chapter 4

## OFDM TRANSMITTER DESIGN

In this project, our main aim is to design a system that can reach the desired performance under experimental conditions. To do so, some practical considerations must be taken into account and, given that information, the implementation is then designed to best perform with the available hardware.

In this chapter, the implemented OFDM system is designed and system model of transmitter is introduced. Also, implementation of transmitter algorithms is explained.

### 4.1 System Model

The model used on the transmitter side consists of a typical OFDM system with  $K$  sub-channels which is designed considering the underwater channel effects. Transmitter system model is shown in Fig 4.1 where  $S/P$  denotes serial-to-parallel conversion.

In the beginning of the transmitter model when data streams that contains information bits are received, they are converted into parallel  $K$  streams which contains  $N_i$  information bits in each.  $N_i$  is defined based on the mapping used in the transmitter. In our system we use Quadrature Phase Shift Keying (QPSK) modulation scheme so  $N_i$  is 2. For doing QPSK mapping,  $K$  mapping blocks are defined, one for each stream as it is shown in 4.1. After mapping the information bits into data symbols, IFFT modulation is handled and data symbols are converted into a time-domain baseband signal. In our system, based on channel needs zero-padded (ZP) - OFDM scheme is used. The reasons behind that decision is detailed in Section 4.2.2. After baseband signal is generated in the previous block, a guard time is inserted to form a ZP-OFDM block. The guard time is a sequence of zeros which has a duration of  $T_g$ .

After guard time is inserted, the frequency adjustment is performed and the signal is shifted to the passband. In our system, we use a center frequency ( $f_c$ ) of 27 kHz and a bandwidth

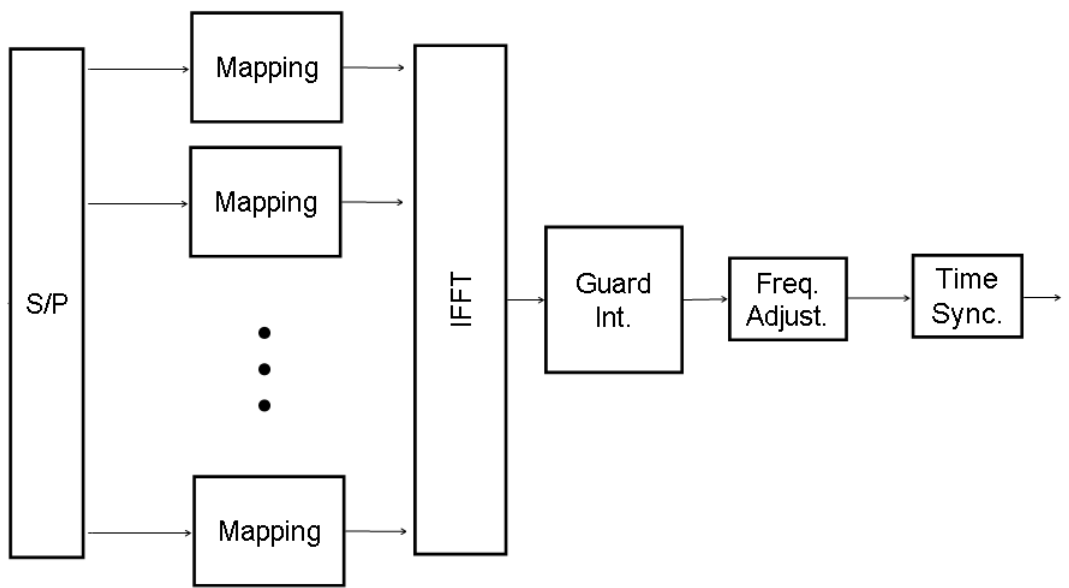


Figure 4.1: Transmitter System Model

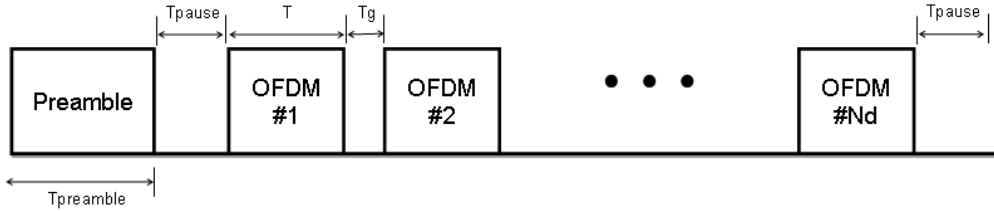


Figure 4.2: Packet Structure

(B) of 12 kHz based on our hardware design constraints which are detailed in Section 5. As a result, a ZP-OFDM block is generated which has duration ( $T$ ) of  $K/B$  and a guard time of  $T_g$ . In a ZP-OFDM block each subcarrier has a frequency spacing of  $\Delta f = 1/T$ , so the  $k$ th subchannel of the block will be;

$$f_k = f_0 + k \cdot (\Delta f) \quad k = 0, \dots, K-1 \quad (4.1)$$

where  $f_0$  denotes the lowest subchannel frequency. The generated ZP-OFDM block at passband is given by;

$$s(t) = \operatorname{Re} \left\{ \left[ \sum_{k=0}^{K-1} s(k) e^{j2\pi k \Delta f t} g(t) \right] e^{j2\pi f_{low} t} \right\}, t \in [0, T + T_g] \quad (4.2)$$

where  $g(t)$  is rectangular pulse shape which has a duration of  $T$  and unit amplitude that defines the zero-padding operation. In addition,  $s(k)$  denotes the data symbol at the  $k$ th subchannel.

In the next step,  $N_d$  ZP-OFDM is generated and a time synchronization preamble is inserted to generate the packet structure which is shown in Fig. 4.2.

$T_{pause}$  which is shown in Fig. 4.2 denotes the pause time of 50ms.

As a result, the transmitted signal is generated as shown in Fig. 4.3.

## 4.2 Implementation of Transmitter Algorithms

In this section, the most important parts of the transmitter algorithms are detailed. In addition, specific information about the theoretical fundamentals are given along with some

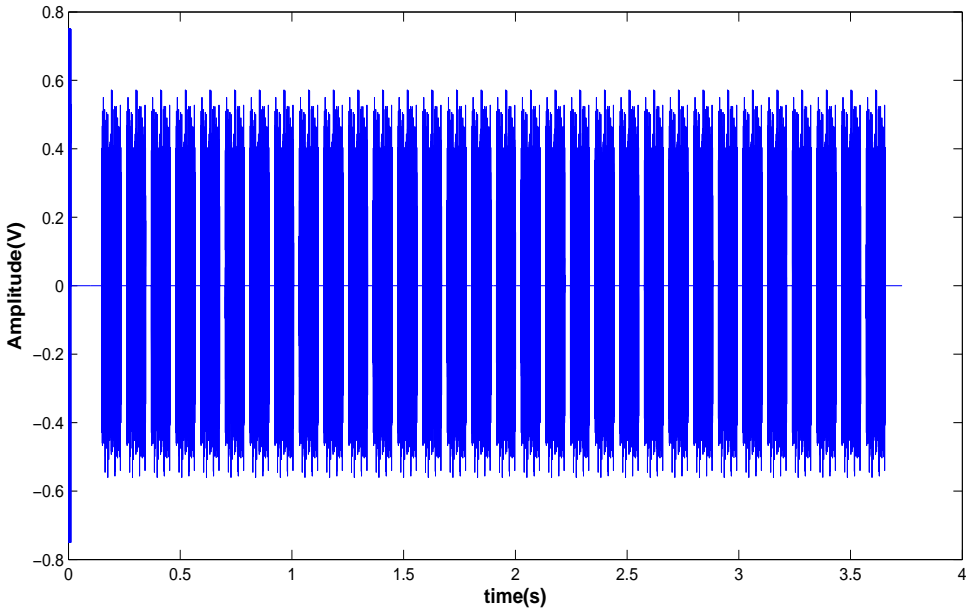


Figure 4.3: Transmitted Signal

practical considerations.

#### 4.2.1 IFFT Modulation

In this block, IFFT modulation is performed according to algorithms in Chapter 3. Additionally, an upsampling operation is performed. This operation is performed for correct demodulation of the OFDM blocks by fulfilling the Nyquist Sampling theorem. Based on that theorem, the sampling frequency  $f_s$  should meet the requirement of  $f_s > 2 \cdot f_h$  where  $f_h$  denotes the higher frequency component in the transmitted signal. Besides that requirement, we consider the idea which is proposed in [13] while determining our systems'  $f_s$ . Selecting  $f_s$  as an integer multiple of bandwidth of the transmitted signal simplifies the upsampling operations at transmitter and downsampling operations at receiver for baseband signal processing. Therefore, we select  $f_s$  as 96 kHz which is an integer multiple of  $B = 12 \text{ kHz}$  and it fulfills the Nyquist sampling theorem as  $f_h = 33 \text{ kHz}$ .

As we select  $f_s$  as 96 kHz, we need to append  $7 \cdot K$  zeros to the end of  $K$  data symbols. As a result, a vector denoted as  $\check{s}$  is generated whose first  $K$  positions are accommodated by data symbols while the other  $7 \cdot K$  spots contain appended zeros. After that,  $N_u$ -point

IFFT is performed as it is shown in Eq. 4.3.

$$u(l) = \sum_{k=0}^{N_u-1} \check{s}(k) e^{j2\pi kl/N_u}, l = 0, 1, \dots, N_u - 1 \quad (4.3)$$

where  $N_u$  denotes the number samples during time  $T$ .

#### 4.2.2 Time Synchronization and Guard Time

Time synchronization is very important because it is used for locating the OFDM blocks for demodulation. Its main job is to provide correct timing for the system to retrieve the data correctly, therefore avoiding inter-block-interference(IBI) or totally wrong detection due to wrong time synchronization.

In our system, time synchronization operation is provided by a preamble. This preamble is a pseudo-random (PN) sequence of length 127, quadrature modulated at the frequency of  $f_c$  and it has a duration of 100 ms. It is also designed to have good correlation properties (only a main peak is the result of an autocorrelation of the modulated synchronization preamble). The preamble is transmitted with the highest power for maximizing the probability of detection.

Guard time is very important for avoiding ISI as it is explained in Chapter 3. As our OFDM transmitter model is designed based on zero-padded (ZP)-OFDM modulation, padded zeros will occur at the guard interval. The reason why we employ ZP instead of cyclic prefixing (CP) is ZP does not spend too much transmission power like CP does and it is more effective than CP in channels which have long delay spreads like underwater channel [16].

# Chapter 5

## OFDM RECEIVER DESIGN

In this chapter, system model of receiver and implemented receiver algorithms are explained.

### 5.1 System Model

The OFDM receiver model is proposed which is shown in Figure 5.1 where BPF and LPF denotes band-pass filtering and low-pass filtering respectively. The receiver model is designed according to underwater acoustic channel effects and transmitted signal properties.

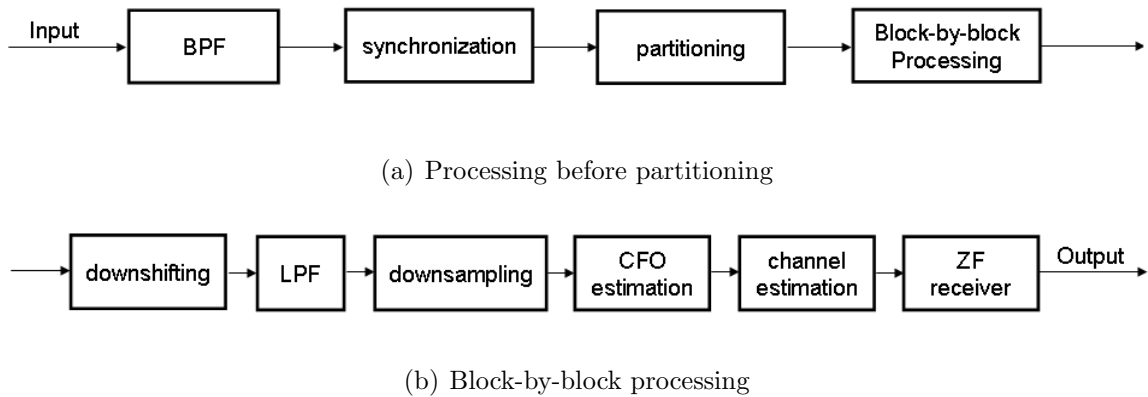


Figure 5.1: Receiver System Model

The proposed receiver model performs processing in discrete-time domain, so the signal is directly sampled with the hardware in the system before doing any processing.

The receiving process begins with band-pass filtering which is performed for minimizing the out-band noise in the received signal. After, time synchronization is performed to receive the OFDM blocks correctly. For that process, cross-correlation operation of known preamble and received preamble is used. This operation is performed for a length of number of samples between the beginning of the preamble and the first OFDM block which is

denoted as  $N_{sync}$ . As it is explained in Section 4.2.2, a high peak occurs as a result of the cross-correlation operation. This peak determines the starting point of the preamble, so correct data reception can be performed. Following time synchronization, the received signal packet is partitioned into OFDM blocks. After that step, all processing is performed at block-by-block basis.

The block-by-block processing starts with a down-shifting operation which converts pass-band signal into a baseband one. After that, a low-pass filtering is performed for having only baseband signal. The baseband signal is down-sampled to a sampling frequency ( $f_s$ ) of 12 kHz before applying the receiver algorithms.

As baseband signal is down-sampled, carrier-frequency-offset (CFO) estimation and compensation operations take place. In this step, we use a low-complex overlap-add(OLA) based demodulation [16] for OFDM. By that operation, received data is converted in frequency domain. In the following step, pilot-tone based channel estimation is performed and data symbols are received by using linear zero-forcing (ZF) receiver as it is shown in (5.1).

$$\hat{s}(k) = (H^H(k)H(k))^{-1}H^H(k)z(k) \quad (5.1)$$

where  $H(k)$  denotes the channel's frequency response on the  $k$ th subchannel.

## 5.2 Receiver Algorithms

In this section, receiver design algorithms are detailed.

### 5.2.1 Pilot Tone based Channel Estimation

Estimating the channel response is a vital part of the receiver as channel frequency response is needed while equalization is being carried out. In our receiver design, channel estimation is performed based on the pilot symbols. According to our design,  $K_p$  symbols of  $K$  data symbols are determined as pilot symbols and they are used in channel estimation. This pilot symbols are determined based on some specifications which minimizes the complexity [14]. These specifications are:

- $K_p$  pilot symbols are chosen equally spaced at subcarriers.

$$0, M, 2M, \dots, (K_p - 1)M, M = K/K_p \quad (5.2)$$

where  $p_1, p_2, \dots, p_{K_p}$  denotes pilot symbols subcarrier indices.

- Pilot symbols are PSK signals that have unit amplitudes.

As pilot symbols are chosen, the channel's frequency response is estimated based on them.

Define:

$$D_s = \begin{bmatrix} s[p_1] \\ \vdots \\ s[p_{K_p}] \end{bmatrix} \quad V = \begin{bmatrix} 1 & e^{-j2\pi p_1/K} & \dots & \dots & e^{-j2\pi p_{K_p}/K} \\ \vdots & \ddots & & & \vdots \\ \vdots & \vdots & \ddots & & \vdots \\ \vdots & \vdots & \vdots & \ddots & \vdots \\ 1 & e^{-j2\pi p_{K_p}/K} & \dots & \dots & e^{-j2\pi p_{K_p}/K} \end{bmatrix}$$

$$h = \begin{bmatrix} h_o \\ \vdots \\ h_L \end{bmatrix} \quad v = \begin{bmatrix} v_{p_1} \\ \vdots \\ v_{p_{K_p}} \end{bmatrix} \quad z_p = \begin{bmatrix} z_{p_1} \\ \vdots \\ z_{p_{K_p}} \end{bmatrix}$$

Channel taps are computed by least-squares (LS) formulation, if  $K_p > L + 1$  where  $L$  denotes channel taps. As a result (5.3) shows LS formulation.

$$z_p = D_s V h + v \quad (5.3)$$

Based on our system properties as pilot symbols are equi-spaced,  $V^H V = K_p I_{L+1}$  [28]. Pilot symbols have unit amplitude, so  $D_s^H D_s = I_{K_p}$  where  $(.)^H$  denotes Hermitian transpose. We can simplify LS formulation into (Eq. 5.4).

$$\hat{h}_{LS} = \frac{1}{K_p} V^H D_s^H z_p \quad (5.4)$$

By using Eq. 5.4, time-domain channel estimation is performed. In the next step, the frequency domain channel estimation can be reached by using time-domain estimation in Eq. 5.5.

$$H(k) = \sum_{l=0}^L h(l)e^{-j2\pi kl/K}, k = 0, \dots, K-1 \quad (5.5)$$

We use LS formulation, so there will be a LS fitting error which can be calculated as,

$$\epsilon_{LS} = \|z_p\|^2 - K_p^{-1} \|V^H D_s^H z_p\|^2 \quad (5.6)$$

### 5.2.2 CFO Estimation

Carrier-frequency-offset (CFO) estimation and compensation is a vital algorithm process for OFDM in a UWA channel. This is because, fast variations in UWA channel cause inter-subcarrier-interference (ICI) and create lost of orthogonality among subcarriers in OFDM blocks. So if CFO compensation is not applied, then ICI severely affects channel estimation and receiver performances. CFO estimation can change from block to block and it is denoted by  $\epsilon$ .

In our receiver, CFO estimation technique in [14] is used. CFO estimation is performed based on the LS fitting error in Eq. 5.6.

CFO estimation can be defined as in matrix form;

$$\Gamma(\epsilon) = \text{diag}(1, e^{j2\pi T_s \epsilon}, \dots, e^{j2\pi T_s \epsilon (K+L_{zp}-1)}) \quad (5.7)$$

where  $L_{zp}$  and  $T_s$  denote number samples (at  $f_s = B$ ) in a guard interval, which is explained in Section 5.1 and  $T_s$  stands for sampling interval that equals to  $T/K$  respectively.

As CFO estimation matrix is defined in Eq. 5.7, a CFO compensation can be made up based on it. This compensation equation also creates input data for pilot-tone based channel estimation block. The equation is;

$$z(\epsilon) = FFT_K(R_{ola}\Gamma(\epsilon)^{-1}y) \quad (5.8)$$

where  $FFT_K$ ,  $y$ ,  $z(\epsilon)$ ,  $R_{ola}$  denote K-point Fast-Fourier Transform, processed signal, created input data for pilot-tone channel estimation and matrix of overlap-adding operation respectively.

The  $R_{ola}$  is a  $KxK + L_{ZP}$  matrix which is equal to  $[I_K, I_{ZP}]$ , where  $I_M$  denotes a  $MxM$  identity matrix.  $R_{ola}$  matrix defines a process of adding last  $L_{ZP}$  entries of the  $y$  to the first  $L_{ZP}$  of it, while holding the first  $K$  entries.

As a result,  $z(\epsilon)$  is formed. By using  $z(\epsilon)$ , we employ LS fitting error with one dimensional search for finding best value for  $\epsilon$ , so a CFO estimator model is formed as it is shown in Eq. 5.9.

$$\hat{\epsilon} = \operatorname{argmin}_{\epsilon} \left\{ \|z_p(\epsilon)\|^2 - K_p^{-1} \|V^H D_s^H z_p(\epsilon)\|^2 \right\} \quad (5.9)$$

# Chapter 6

# EXPERIMENT SETTING

Following successful completion of simulations, we tested our system in the underwater channel. Experiment setting along with the hardware are selected in a way to have the optimal performance while data rate and useful bandwidth are used at maximum.

## 6.1 Deployment

ZP-OFDM signals have been transmitted and collected in several experiments at Bilkent Lake Facility, Ankara. Photo of Bilkent Lake Facility can be seen in Fig. 6.2 . We will present some results regarding the experiment performed Bilkent Lake Facility, Ankara in June 2011. The transmission range was 7 m . The transmitter and receivers were anchored about 5 m in shallow water.

The bottom profile of Bilkent Lake is not flat, it has an increasing depth from the shore, and due to the platform on the water, there are multiple reflections from the shore and buoys.

The experiment setup can be seen in Fig. 6.1 .

The illustrative block diagram for the underwater tests is shown in Fig. 6.3 for the transmitter (left), and for the receiver(right)

## 6.2 Hardware

- **Laptop**

The transmitting side laptop is used to generate data with MATLAB. A C++ script is used to transmit the data to the NI USB-6251 BNC DAQ Card and from it to the transmitting hardware, which in this case is the Krohn-Hite Model 7500 Power Amplifier coupled with the transducer by an impedance matching transformer. On

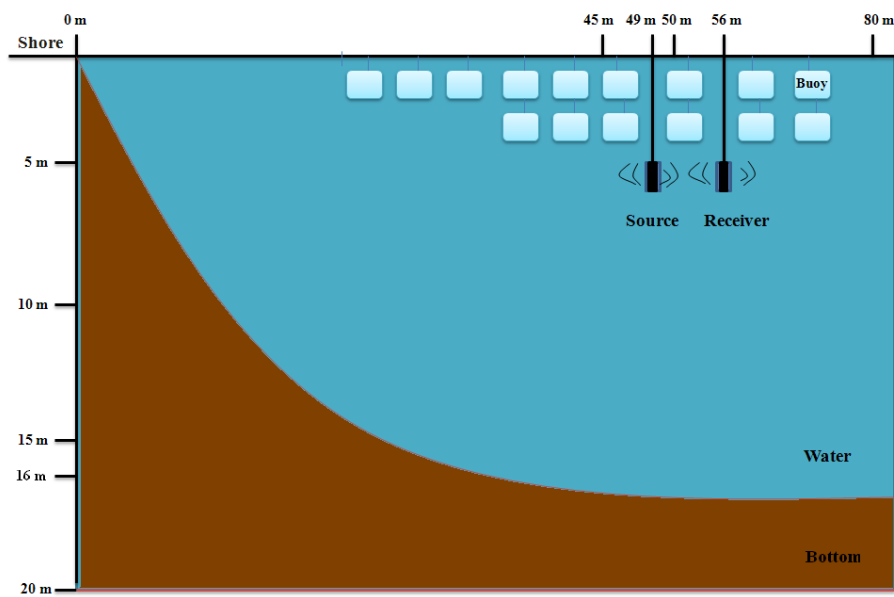


Figure 6.1: Experimental Setup



Figure 6.2: Bilkent Lake Facility

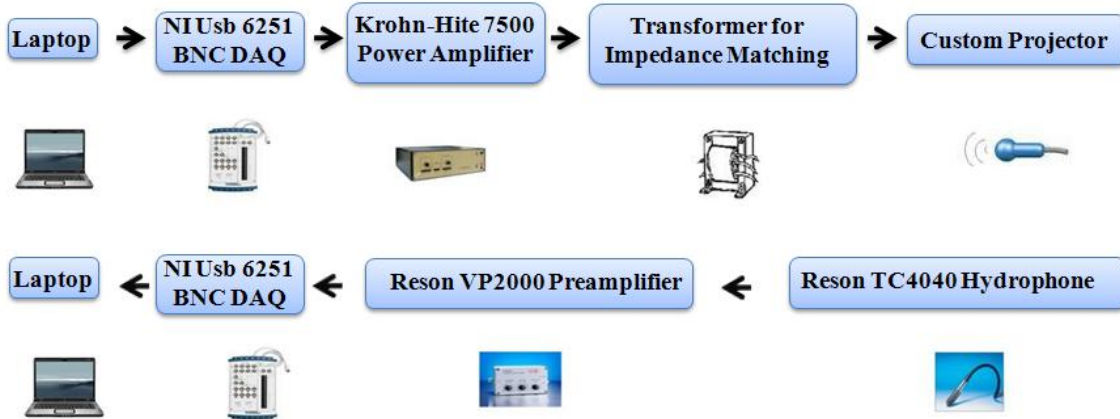


Figure 6.3: Transmission block diagram for underwater tests, transmitter(up) and receiver(bottom)

the receiving side, the laptop receives the data from the USB-6251 BNC DAQ Card via another C++ script and the demodulation is performed.

- **National Instruments USB-6251 BNC Data Acquisition(DAQ) Card**

NI USB-6251 BNC Data Acquisition(DAQ) Card is used as an interface that allows the transmission of the generated acoustic signals by sampling the analog signal at 96 kHz provided by the laptop computer.

- **Krohn-Hite Model 7500 Power Amplifier**

The signal transmitted by the NI USB-6251 BNC DAQ Card is further amplified by the Krohn-Hite Model 7500 Power Amplifier, to adjust the signal power to the transmission requirements in the underwater channel. The power response of the Krohn-Hite Model 7500 Power Amplifier, is shown in Fig. A.1 in Appendix A .

- **Impedance matching circuitry**

Prior to sending the signal to the transducer, an impedance matching transformer adjusts the signal for maximum power transmission to the transducer.

- **Custom Transducer**

Transmitting Voltage Response (TVR) of the transducer is 130 dB at resonance frequency. Transducer is omnnidirectional. The response has a resonance frequency, and

it decays at lower and higher frequencies, thus limiting the transmission bandwidth to about 12 kHz.

- **Reson TC400 Hydrophone**

Reson TC400 ideal standard reference hydrophone has been chosen for the reception of the acoustic OFDM signal. Its most important characteristic is the wide frequency range and the relatively high transmitting sensitivity. The horizontal directivity pattern and receiving sensitivity is provided in Fig. A.2 in Appendix A .

- **Reson VP2000 Preamplifier**

Once the signal is picked up by the hydrophone, the Reson VP2000 preamplifier amplifies and filters the received signal. The characteristics of the high-pass and low-pass filters are given in Fig.A.3 in Appendix A. As it can be seen, the filter response is adjustable depending on the signal frequency components.

- **National Instruments USB-6251 BNC Data Acquisition(DAQ) Card**

NI USB-6251 BNC Data Acquisition(DAQ) Card is also used as an interface that allows the reception of the generated acoustic signals by sampling the analog signal at the desired rate(96 kHz) provided by the Reson VP2000 preamplifier, and transmitting it to the receiving laptop.

# Chapter 7

## RESULTS ON EXPERIMENTAL DATA

In order to verify the operation of our modem, we first tested the analog components and digital components separately and then tested the full, integrated system at Bilkent University Lake Facility. This chapter describes the results of each test and summarizes the performance of our modem and comparisons are made with some existing systems in literature.

### 7.1 Simulation Tests

Simulation tests are performed by using the proposed system model which is explained in previous chapter. By using these test results, we are able to understand the system performance and its' characteristics before testing it in a real underwater channel. In this thesis, we use Bellhop model for simulating UWA Channel. The reason why we use Bellhop is that it is accurate and suitable to model high-frequency acoustic propagation in shallow water. Further explanation about Bellhop can be found in Appendix B. Bellhop mainly works on ray tracing. In Figure 7.1, a Bellhop ray tracing model for a 27 kHz source with a 180 degree beam angle placed at 5 meters in a isothermal body of water 16 meters deep with sound speed of 1512 m/s can be observed. By using ray path knowledge, the Bellhop model calculates the transmission loss by using the pressure fields, therefore we add real underwater noise field to the signal which is recorded in Bilkent Lake Facility. As a result, we have a simulator system model which is shown in Figure 7.2.

The properties of the simulator should be identified well in order to build a correct configuration. In the simulator, time variation, which is a characteristic of underwater channel and hardware effects are not considered. As a result, the achieved performance for the

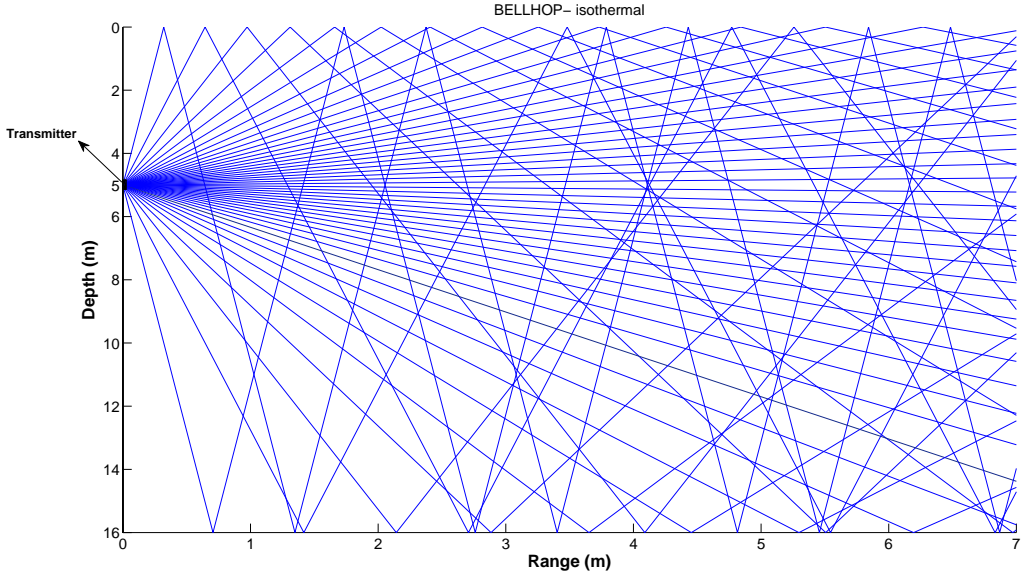


Figure 7.1: Bellhop Ray Tracing

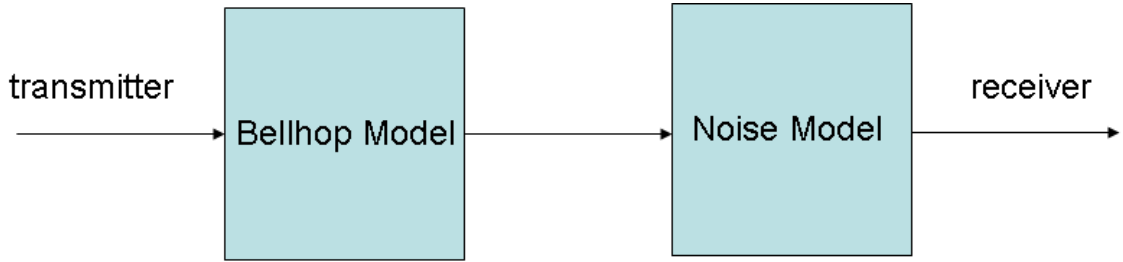


Figure 7.2: System Model of the Simulator

simulated data is much better than the one for the real underwater channel.

In the simulation tests, the same OFDM parameters and packet structure used in experiments are used, as shown in Table 7.1.

In the first simulation we use the system deployment which is shown in Fig. 7.3. In this system, projector has a directivity and radiates at 180 degree towards to receiver. Figure 7.4 shows the constellation plot of the received symbols. The bit-error-rate(BER) is 0 for each OFDM block. The estimated channel response by using PN sequence preamble matching is shown in Figure 7.5.

As we can observe from the channel response in Figure 7.5, the delay spread of the channel is shorter than the guard interval time 25 ms. So this means, there is no inter-block

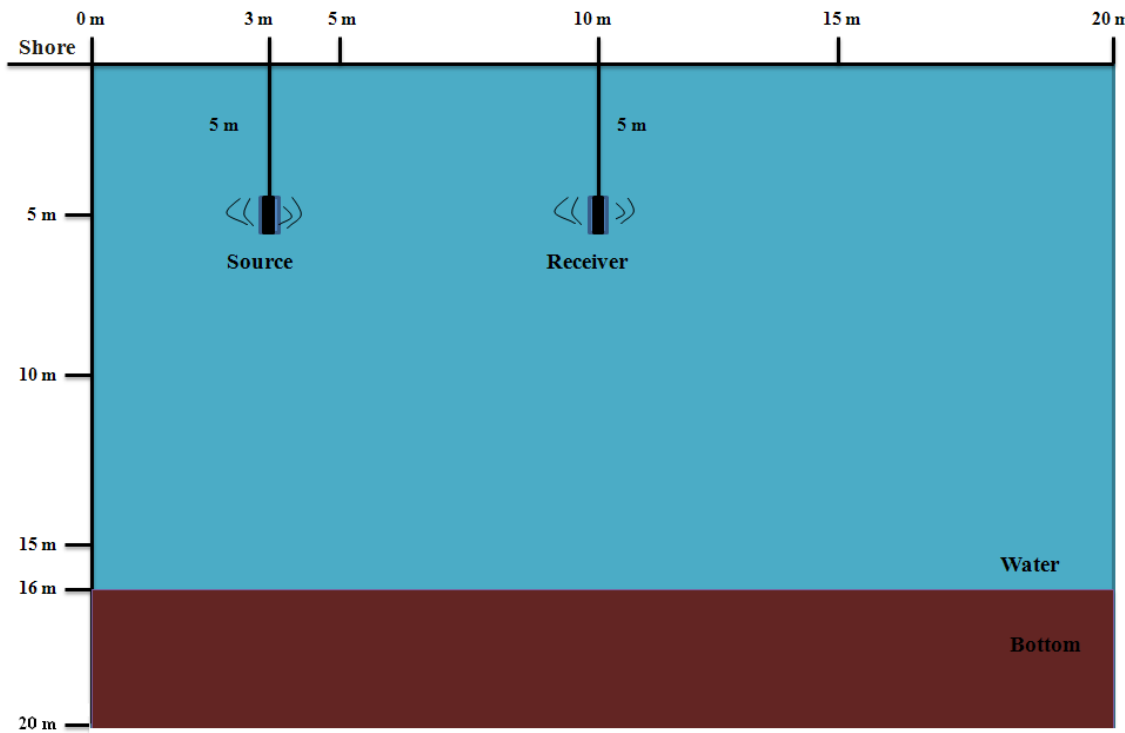


Figure 7.3: Simulation setup

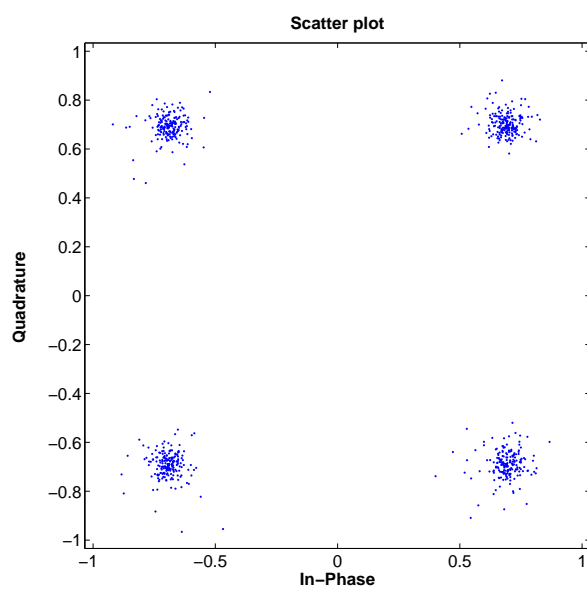


Figure 7.4: Received QPSK constellations of OFDM blocks

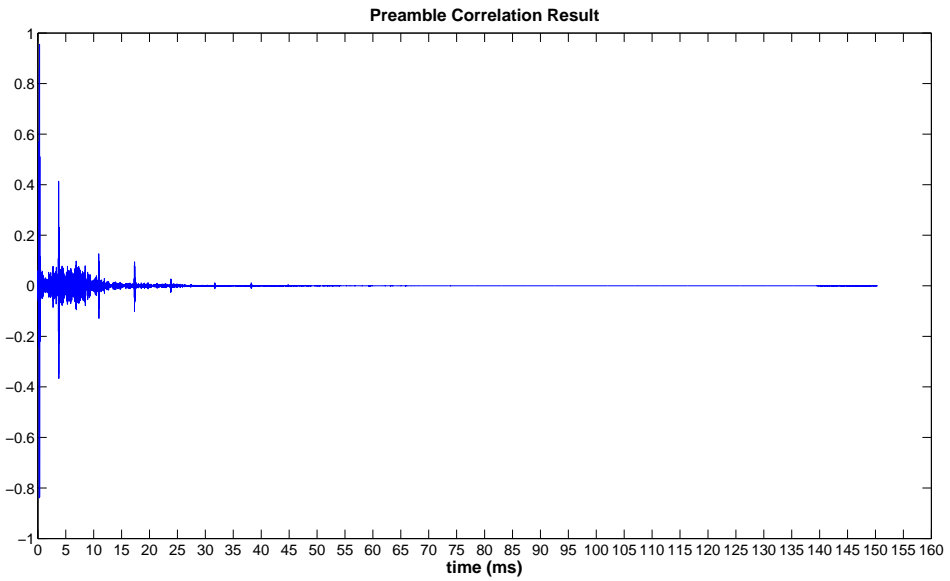


Figure 7.5: Estimated Channel Response by suing PN sequence matching

interference(ICI) in the received signal.

The first simulation is performed for a similar system deployment with our system, but it does not include the shore in our system deployment which is shown in Figure 6.3. Therefore, for better interpretation of our system, we decided to add shore reflections in our simulations, but we can not do that by using Bellhop model. The Bellhop model is not able to simulate a 360 degree(omni-directional) signal, so we simulated shore effect by calculating these paths externally and adding them on the bellhop model results. Some of these paths are shown in Figure 7.6. The duration of the paths varies between 25 ms and 140 ms.

Figure 7.7 shows constellation plot of the received symbols. From Figure 7.8, it can be seen that BER is around  $10^{-2}$ . The estimated channel response by using PN sequence preamble matching is shown in Figure 7.9.

As we can observe from the channel response in Figure 7.5, the delay spread of the channel is longer than the guard interval time 25 ms. So this means, IBI occurs in the received signal. When the delay spread is longer, BER performance gets worse. Therefore, we can say that IBI severely effects BER performance.

By doing simulations, we are able to see our system performance in a similar environment

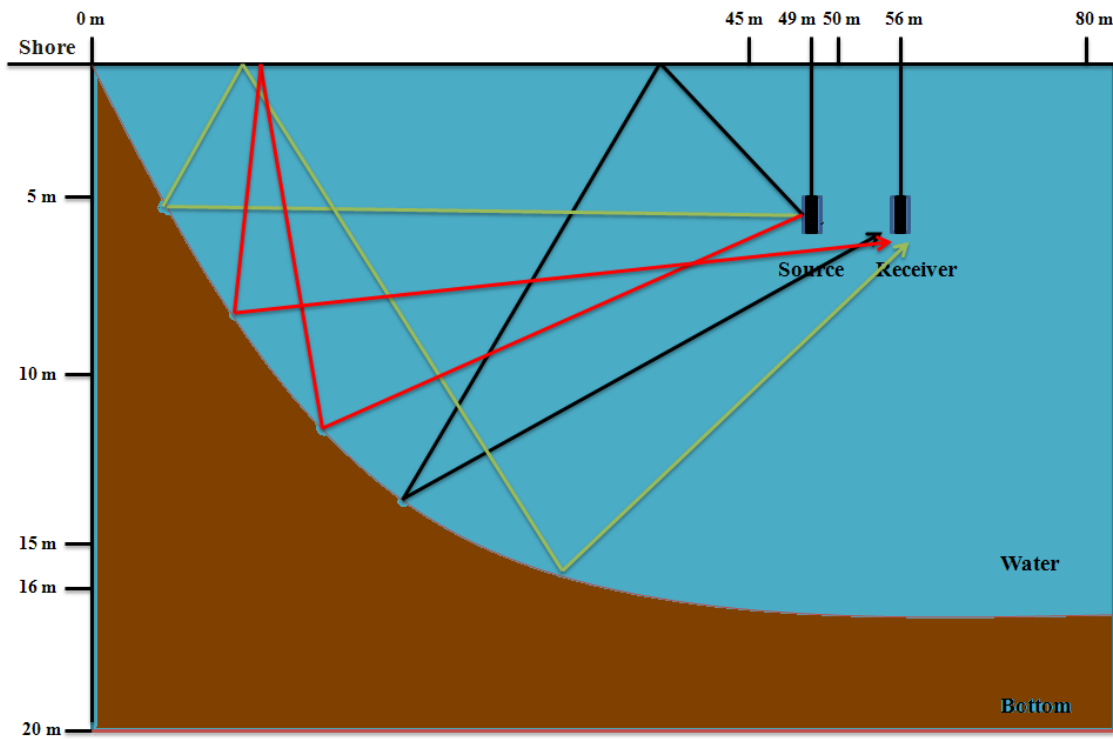


Figure 7.6: Ray paths which come from the shore reflection

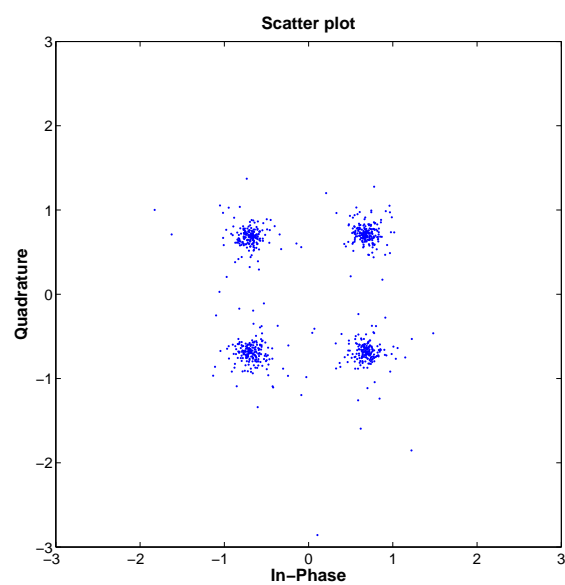


Figure 7.7: Received QPSK constellations of OFDM blocks

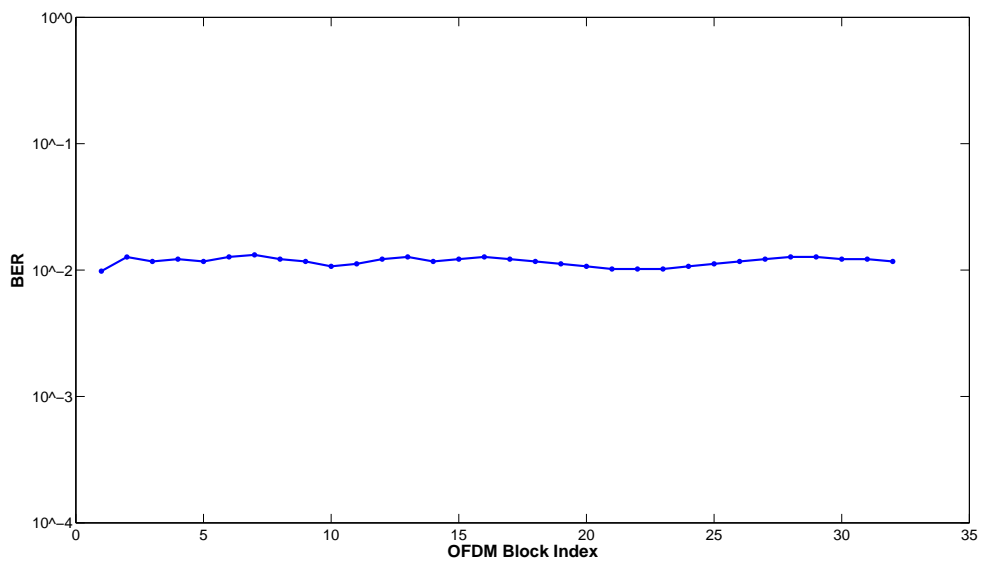


Figure 7.8: BER for each OFDM block in a packet

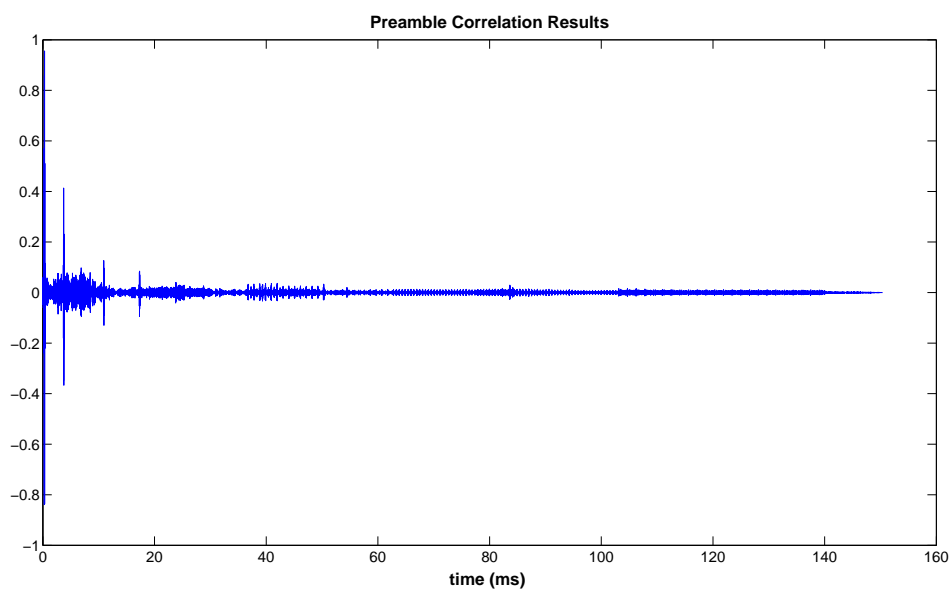


Figure 7.9: Estimated Channel Response by suing PN sequence matching

to our experimental environment. As a result, we can understand and analyze future experimental results better.

## 7.2 Underwater Experiment

The underwater experiments are performed by using the system deployment detailed in Chapter 6. The OFDM parameters that are used for the underwater tests are summarized in Table 7.1 for one ZP-OFDM block.

Table 7.1: System Parameters of ZP-OFDM block

Center frequency	$f_c = 27 \text{ kHz}$
Signal Bandwidth	$B = 12 \text{ kHz}$
OFDM block duration	$T = 85.33 \text{ ms}$
Guard Time	$T_g = 25 \text{ ms}$
Subcarrier spacing	$\Delta f = 11.72 \text{ Hz}$
number of subcarriers	$K = 1024$
number of data subcarriers	$K_d = 768$
number of pilot subcarriers	$K_p = 256$

For our system the data rate is:

$$R = \left(2B \frac{T}{T + T_g}\right) \left(\frac{K - K/4}{K}\right) = 13.92 \text{ kbps} \quad (7.1)$$

In experiments we use the packet structure shown in Fig. 4.2 and we choose  $N_d$  as 32. Therefore, our system has 32 OFDM blocks and 32768 data symbols per packet.

Received signal which is shown in Fig. 7.10, is directly analog-to-digital converted and all processing operations are performed at discrete-time. In the following subsections, processing results of the received signal are proposed and analyzed.

### 7.2.1 CFO and Channel Estimation

CFO estimation is done on a block-by block basis, as detailed in Sec. 5.2.2

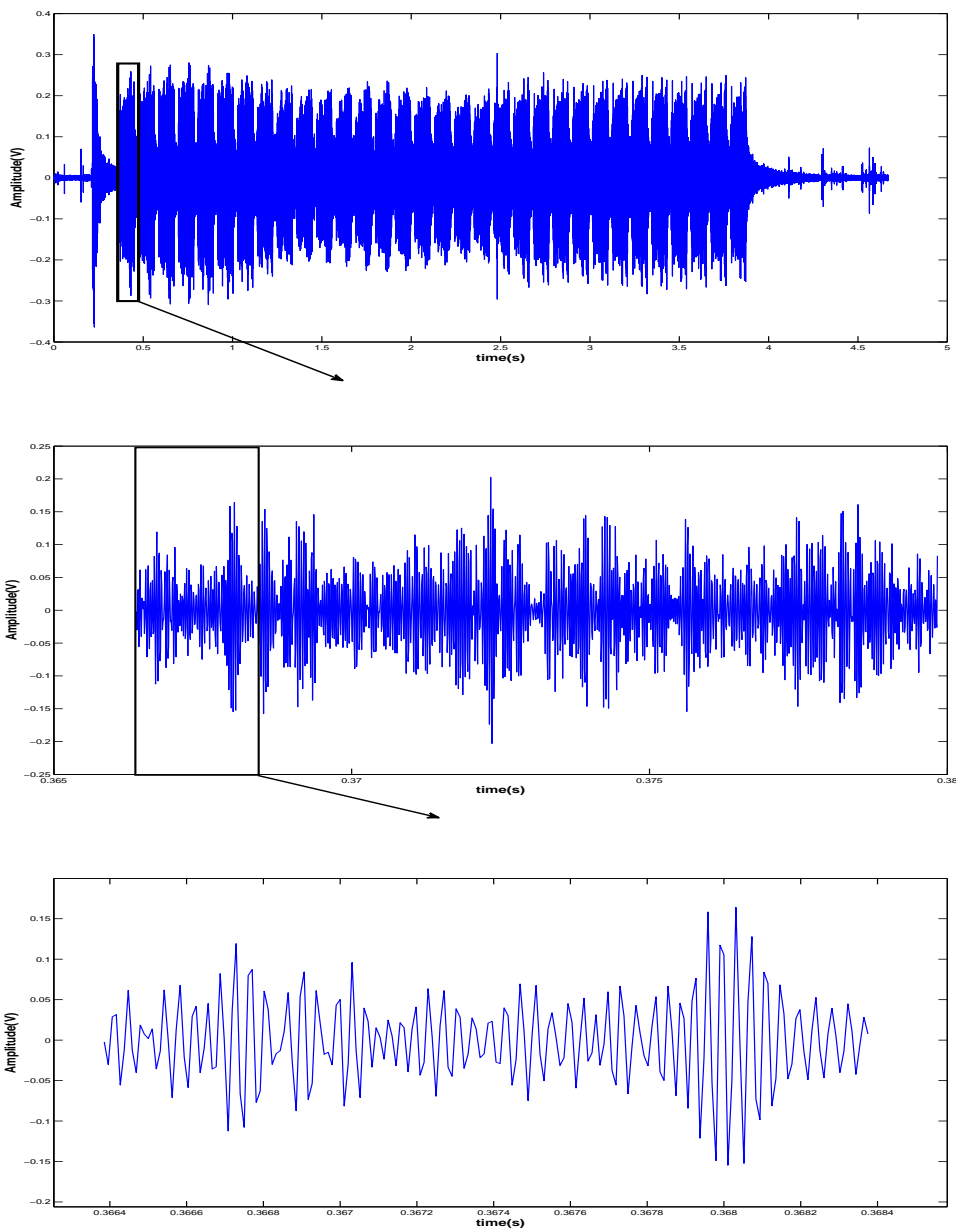


Figure 7.10: Received Signal

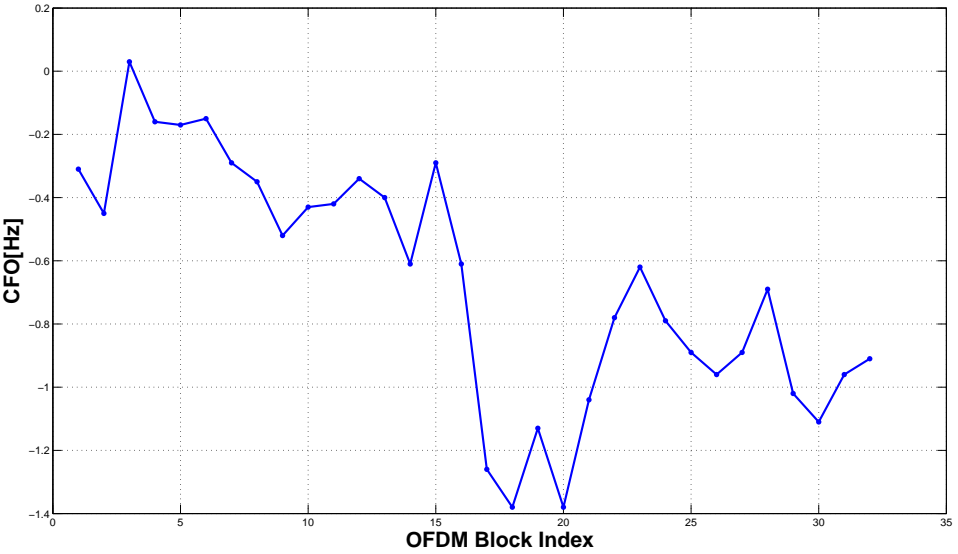


Figure 7.11: CFO Estimation

Fig. 7.11 shows the CFO estimates for each block separately , where  $K = 1024$  and each packet has 32 OFDM blocks. We observe that the CFO changes from block to block roughly but cannot be regarded as constant. Without the CFO fine tuning, the receiver does not work and performance may be severely effected by(ICI).

CFO is within  $[-1.4,0]$  Hz range, which may be caused by transmitter and receiver drifting with small waves. These CFO estimates can be treated as Doppler shift and they can be translated into moving speeds that vary between 0 and 0.078 m/s (or 0 and 0.151 knots). With  $K_p = K/4 = 256$  equi-spaced subcarriers, channel estimation for 32 blocks are shown in Fig. 7.12 .

Since  $K_p = K/4 = 256$  pilots tones are used for each channel estimation, our design can only handle channels with at most  $L+1 = 256$  taps.

Path 1 : There is a strong direct path between the transmitter and the receiver.

Path 2 : A second path is also observed in Fig. 7.12 . We conjecture that this path is from the surface bounce. This conjecture is supported by a rough computation based on the channel geometry.

Direct path distance is 7 m and the depth is 5 m. Then, the delay between the surface bounce and the direct path is

$$\left(2 \times \sqrt{(3.5)^2 + 5^2} - 7\right) / 1500 = 3.47ms$$

Path 3: A third path is also observed in Fig. 7.12 . We conjecture that this path is from the bottom bounce. The depth of the bottom is roughly 11 m from both receiver and transmitter. Then, the delay between the surface bounce and the direct path is

$$\left(2 \times \sqrt{(3.5)^2 + 11^2} - 7\right) / 1500 = 10.73ms$$

Path 4: A third path is also observed in Fig. 7.12 . As the path is strong, we conjecture that this path is a combination of surface bounce-bottom bounce and bottom bounce-surface bounce paths. Then, the delay between this pat and the direct path is

$$\left(2 \times \sqrt{(0.887)^2 + 5^2} + 2 \times \sqrt{(2.613)^2 + 11^2} - 7\right) / 1500 = 17.18ms$$

These numbers roughly correspond to the inter-arrival times marked in Fig. 7.12

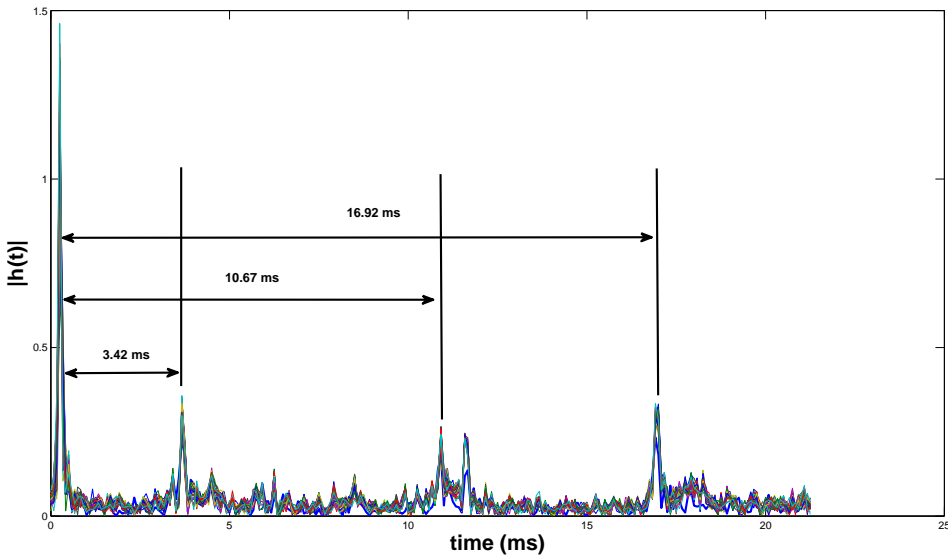


Figure 7.12: Channel Estimation for all blocks

## 7.2.2 BER Performance

Constellation of received signal is shown in Fig. 7.13 .

Following CFO and channel estimation, now we report the bit error rate (BER) performance.

BER performance for each OFDM block in one packet can be seen in Fig. 7.14 . BER varies between  $10^{-2}$  and  $10^{-1}$ where the highest BER is  $9.10^{-2}$  . We emphasize that with

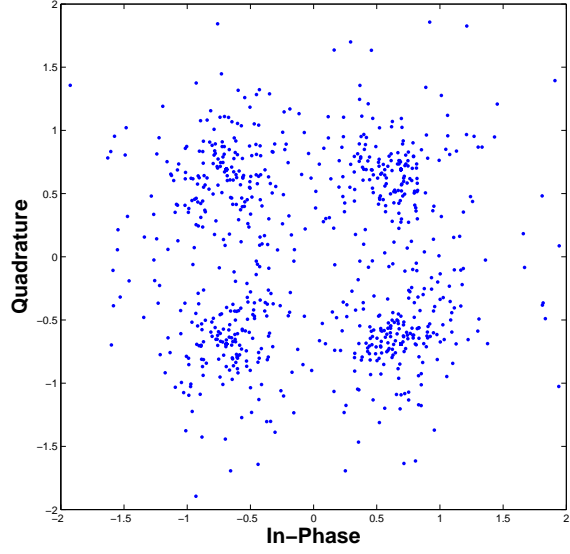


Figure 7.13: Scatter plot for received QPSK signals

block-by-block processing, decoding errors in previous blocks have no impact on future blocks, as confirmed by Fig. 7.14 .

When we examine the BER performance of [14], where we adapted our system from, we see that it is on the order of  $10^{-2}$  and  $10^{-3}$ .

Comparing [14] with our system , one can say that [14] has a better performance by means of BER. However, the main reason behind the difference in BER performance is different environmental conditions.

In [15] ,a comparison between BER performance of a system in two different environmental conditions is made. BER performance under long delay spread and short delay spread is compared. Especially when the delay spread is longer than the guard interval, severe IBI occurs and this affects BER performance adversely. Although BER performance for experiment with long delay spread is not enough, in the article they did not try the channel shortening approach to reduce the IBI before OFDM demodulation (e.g., using methods from [29] [30] [31] ). Instead, they treat all multipath returns after the guard interval as additive noise; hence, the system is operating at low signal-to-noise ratio (SNR). By using channel coding and multichannel reception they improve their performance.

For our case, the channel condition is very difficult with strong multipath after the guard

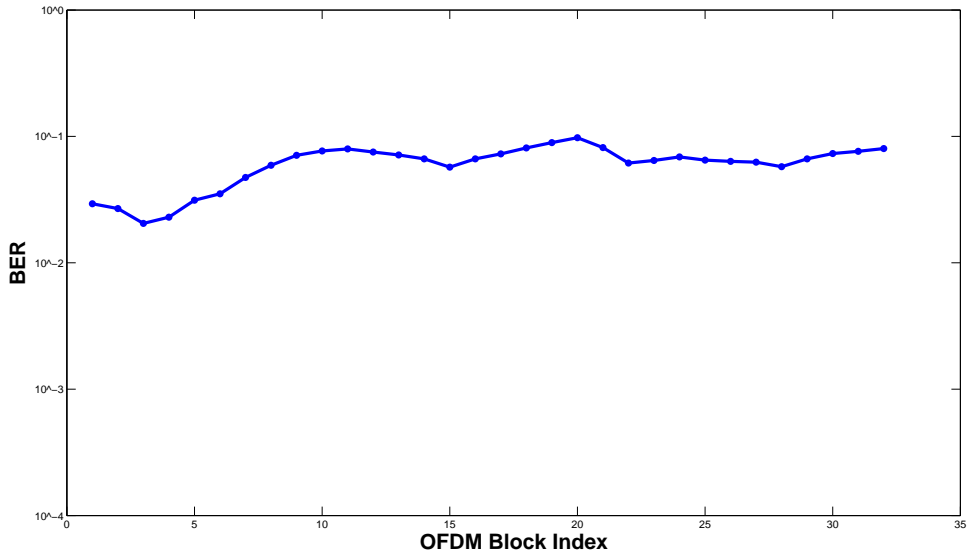


Figure 7.14: BER for each OFDM block in a packet

interval of 25 ms. In order to observe these paths, we obtained channel response estimates by PN sequence preamble matching as discussed in Sec. 5. The last strong path is evident at about 100ms, as shown in Fig. 7.15. This long delay spread is likely due to the reflections off the pilings near the shore with our projector being omni-directional. Some of these reflections can be seen in Figure 7.6. With the channel delay spread longer than the guard interval, IBI emerges and weakens BER performance.

Whereas in [14], delay spread is 6.25ms because experiment was performed at deep water with 2.5 km range. With the channel delay spread shorter than the guard interval, IBI doesn't exist.

As a result, using the comparison in [14] , we can say that as our delay spread which is on the order of 120ms is longer than the guard interval, we have severe BER performance due to IBI whereas for [14], with the channel delay spread of 6.25ms shorter than the guard interval, BER is low.

For our case, SNR is 30 dB whereas SINAD when IBI exists is 10 dB. This is because we treat all multipath returns after the guard interval as additive noise; hence, the system is operating at low SINAD as in [15] because multipath spread is longer than guard interval. As SINAD decreases, BER rate increases.

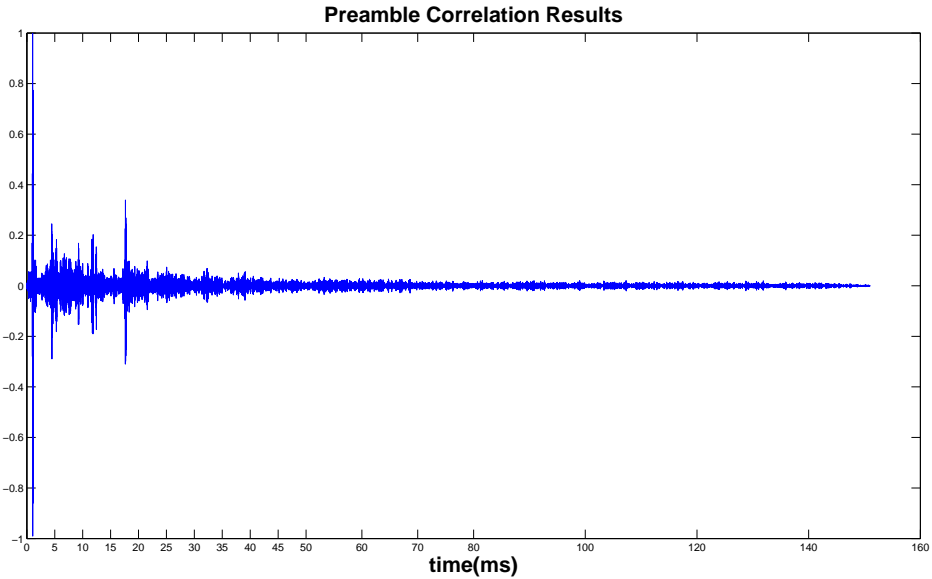


Figure 7.15: Estimated Channel response by using PN sequence matching

Considering the points above, although our BER performance is worse than [14], this is because of different environmental conditions. By doing the tests with the same conditions of [14], our BER would have been on the order of  $10^{-2}$  and  $10^{-3}$ . As a result we have reasonable results.

In addition to the experiments, simulations are done using Bellhop Channel model in underwater channel as detailed in Section 7. The results presented also prove that when the delay spread is longer than guard interval, IBI occurs, so the BER performance gets worse. If our environment did not contain a shore or if we have used a directional projector, then we could have lowered delay spread and improved BER performance.

Based on simulations, experimental results and explanations reached in [15], we reach that our systems BER performance is worse than system BER performance in [14] due to our long channel delay spread. This long delay spread is caused by the receiver and transmitter deployments and environmental properties. As a result we can say that, if our system tests were conducted at the same environment in [14], then our systems' BER performance would have reached the proposed values in the article.

As a result, our system has a BER less than  $9 * 10^{-2}$  and has 13.92 kbps data rate without any coding.

# Chapter 8

## CONCLUSIONS

This thesis describes the design, simulation and testing of a pilot-tone based ZP-OFDM(Zero Padded- Orthogonal Frequency Division Multiplexing) receiver, where CFO(Carrier Frequency Offset) compensation, channel estimation, and data demodulation are carried out on the basis of each OFDM block.

The receiver was tested by simulations using Bellhop UWA(Underwater Acoustic) Channel model in order to investigate the system characteristics before underwater experiments.

The method was tested in a shallow-water experiment at Bilkent Lake. Over a bandwidth of 12 kHz, the data rate was 13.92 kb/s with QPSK modulation , when the number of subcarriers was 1024. Bit-error-rate (BER) was less then  $9 \times 10^{-2}$  without using any coding. BER for the simulation was higher as we eliminated the reflections from the shore.

Future work includes

- use coding to improve BER performance of the system [32].
- shortening methods for channels whose delay spread is longer than the guard interval.
- advanced receiver design, where channel estimation and data demodulation are iteratively coupled. This can further improve the BER performance and also reduce the number of pilots needed [32], [33].
- better modeling of channel variation. Now we have modeled the channel variation within each OFDM block by one CFO variable. We could use multiple CFOs for different portions of the channel taps [33].
- multichannel combining [34], [5], [15].
- adapt the system to deal with non-uniform doppler shift when present [15].
- multiple-inputmultiple-output (MIMO) techniques.

- more experiments with different UWA channels .

# APPENDIX A

## Datasheets

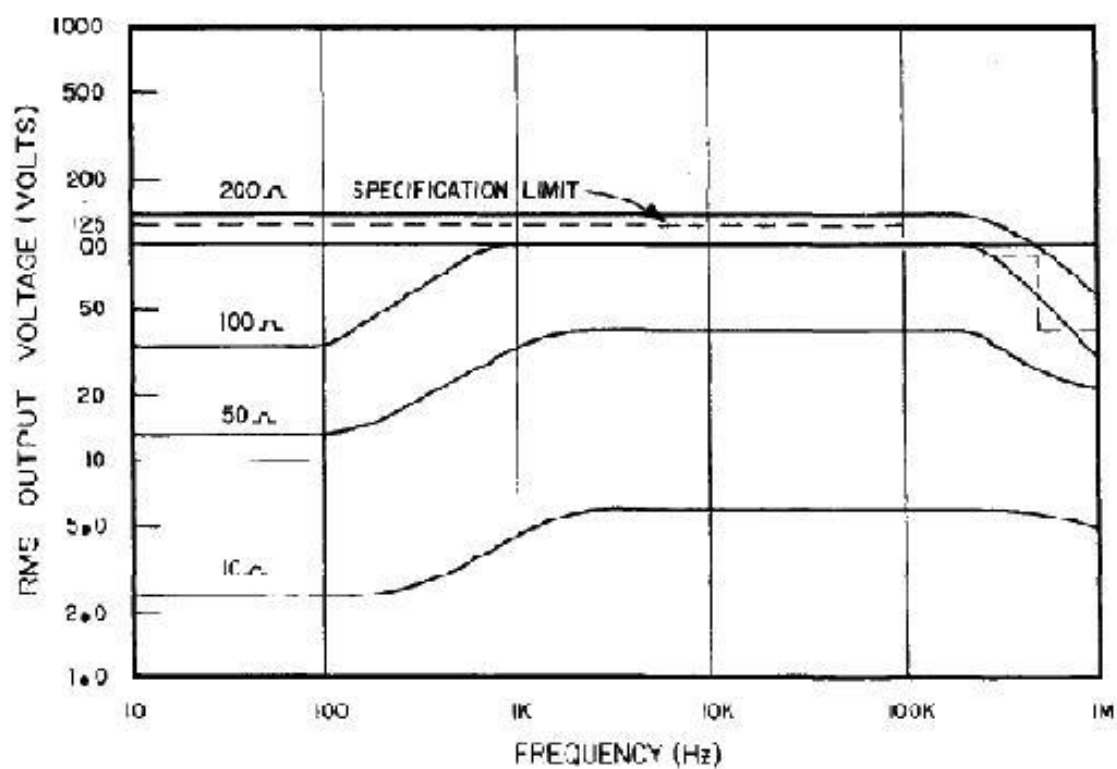


Figure A.1: Power response of the Krohn-Hite Model 7500 Power Amplifier

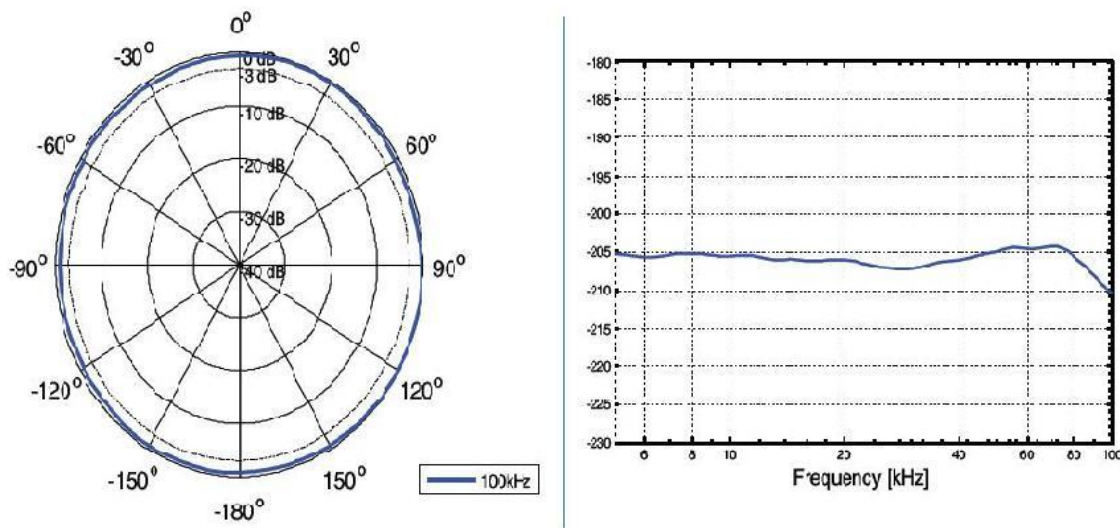


Figure A.2: Horizontal directivity pattern (left) and receiving sensitivity (right) of the Reson TC4040 hydrophone

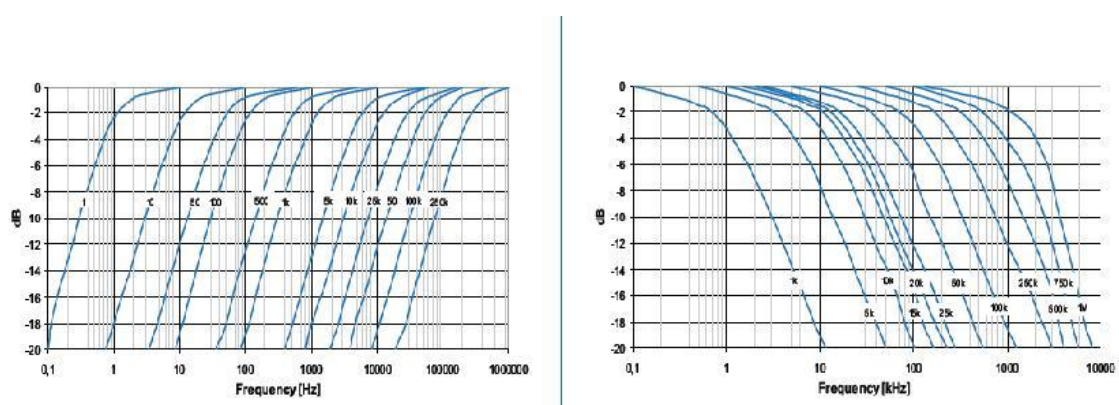


Figure A.3: High-pass filter (left) and low-pass filter (right) frequency responses of the Reson VP2000 preamplifier

## APPENDIX B

# Description of Bellhop Underwater Channel Model

We model the underwater acoustic communication channel using the Bellhop Gaussian beam tracing propagation model. The model, developed in 1987 by Porter and Bucker at the Space and Naval Warfare Systems Center in San Diego, has since been migrated into a MATLAB graphical user interface (GUI) available from the Centre for Marine Science and Technology at the Curtin University of Technology at Perth, Australia [35]. The interface allows users to model multiple layers of water and sediment, each with its own set of unique environmental parameters, such as the sound-speed profile (SSP), density, and root-mean-square (RMS) roughness. The model is capable of producing channel impulse responses, ray traces, source-to-receiver eigenrays, and two dimensional transmission loss plots. Bellhop is designed in order to perform two-dimensional acoustic ray tracing for a given sound speed profile  $c(z)$  or a given sound speed field  $c(r; z)$ , in ocean waveguides with flat or variable absorbing boundaries. Output options include ray coordinates, travel time, amplitude, eigenrays, acoustic pressure or transmission loss (either coherent, incoherent or semi-coherent). The calculation of acoustic pressure is based on the theory of Gaussian beams.

# References

- [1] L. Freitag, M. Grund, J. Preisig, and M. Stojanovic, “Acoustic communications and Autonomous Underwater Vehicles,” *J. Acoust. Soc. Am.*, vol. 115, p. 2620, May 2004.
- [2] I. F. Akyildiz, D. Pompili, and T. Melodia, “Challenges for efficient communication in underwater acoustic sensor networks,” *ACM SIGBED Review*, vol. 1, July 2004.
- [3] J. Cui, J. Kong, M. Gerla, and S. Zhou, “Challenges: Building scalable mobile underwater wireless sensor networks for aquatic applications,” *IEEE Network special issue on Wireless Sensor Networking*, May 2006.
- [4] D. B. Kilfoyle and A. B. Bagheroer, “The state of the art in underwater acoustic telemetry,” *IEEE Journal of Oceanic Engineering*, vol. 25, no. 1, p. 427, 2000.
- [5] M. Stojanovic, J. Catipovic, and J. Proakis, “Adaptive multichannel combining and equalization for underwater acoustic communications,” *Journal of the Acoustical Society of America*, vol. 94, pp. 1612–1631, September 1993.
- [6] A. Doufexi, S. Armour, M. Butler, A. Nix, D. Bull, J. McGeehan, and P. Karlsson, “A comparison of the HIPERLAN/2 and IEEE 802.11a wireless LAN standards,” *IEEE Communications Magazine*, vol. 40, pp. 172–180, May 2002.
- [7] “IEEE standard for local and metropolitan area networks part 16: air interface for fixed broadband wireless access systems,” 2002.
- [8] S. Ahmadi, “An overview of next-generation mobile WiMAX technology,” *IEEE Communications Magazine*, vol. 47, pp. 84–98, June 2009.
- [9] E. Bejjani and J. C. Belfiore, “Multicarrier coherent communications for the underwater acoustic channel,” in *IEEE Oceans’06 Conference*, pp. 1125–1130, September 2006.

- [10] W. K. Lam and R. F. Ormondroyd, “A coherent COFDM modulation system for a time-varying frequency-selective underwater acoustic channel,” in *7th International Conference on Electronic Engineering in Oceanography*, pp. 198–203, June 1997.
- [11] W. K. Lam, R. F. Ormondroyd, and J. J. Davies, “A frequency domain adaptive coded decision feedback equalizer for a broadband UWA COFDM system,” in *OCEANS*, pp. 794–799, Oct. 1998.
- [12] Y. V. Zakharov and V. P. Kodanov, “Multipath-doppler diversity of ofdm signals in an underwater acoustic channel,” *Proc. of ICASSP*, vol. 5, p. 29412944, June 2000.
- [13] M. Stojanovic, “Low complexity OFDM detector for underwater acoustic channels,” in *Proc. of the IEEE Oceans’06 Conference*, (Boston, MA), September 2006.
- [14] B. Li, S. Zhou, M. Stojanovic, and L. Freitag, “Pilot-tone based ZP-OFDM demodulation for an underwater acoustic channel,” in *IEEE Oceans’06 Conference*, (Boston, MA), September 2006.
- [15] B. Li, S. Zhou, M. Stojanovic, L. Freitag, and P. Willett, “Multicarrier communication over underwater acoustic channels with nonuniform doppler shifts,” *IEEE Journal of Oceanic Engineering*, vol. 33, pp. 198–209, April 2008.
- [16] B. Muquet, Z. Wang, G. B. Giannakis, M. de Courville, and P. Duhamel, “Cyclic Prefix or Zero-Padding for Multi-Carrier Transmissions?,” *IEEE Trans. on Communications*, vol. 50, pp. 2136–2148, Dec. 2002.
- [17] “Bellhop gaussian beam/finite element beam code.”
- [18] R.Urick, *Principles of Underwater Sound*. McGraw-Hill, NY, 1983.
- [19] M. A. Ainslie and J. G. McColm, “A simplified formula for viscous and chemical absorption in sea water,” *Journal of the Acoustical Society of America*, vol. 103, no. 3, pp. 1671–1672, 1998.
- [20] B. Benson, *Design of a Low cost Underwater Acoustic Modem for Short Range Sensor Networking Applications*. PhD thesis, UCSD, 2010.

- [21] L.Berkhovskikh and Y.Lysanov, *Fundamentals of ocean acoustics*. Springer, NY, 1982.
- [22] M. Stojanovic, “Underwater acoustic communications: Design considerations on the physical layer,” *Fifth Annual Conference on Wireless on Demand Network Systems and Services, 2008. WONS 2008*, 2008.
- [23] F. Tong, B. Benson, Y. Li, and Kastner, “Channel equalization based on data reuse lms algorithm for shallow water acoustic communication,” *IEEE International Conference on Sensor Networks, Ubiquitous, and Trustworthy Computing*, 2010.
- [24] R. Coates, *Underwater acoustic systems*. Wiley, NY, 1989.
- [25] N. R. C. (NRC), *Ocean Noise and Marine Mammals*. National Academies Press, 2003.
- [26] M. Stojanovic, “On the relationship between capacity and distance in an underwater acoustic communication channel,” *Proceedings of First ACM International Workshop on Underwater Networks*, 2006.
- [27] G. Andrews, A. Ghosh, and R. Muhammed, *Fundamentals of WiMAX understanding broadband wireless networking*. Prentice Hall, 2007.
- [28] J. Rinne and M. Renfors, “Pilot spacing in orthogonal frequency division multiplexing systems on practical channels,” *IEEE Trans. Consumer Electron.*, vol. 42, pp. 959–962, Nov. 1996.
- [29] R. Martin and C. Johnson, “Adaptive equalization transitioning from single carrier to multicarrier systems,” *IEEE Signal Process Magazine*, vol. 22, pp. 108–122, Nov 2005.
- [30] J. Kleider and X. Ma, “Adaptive channel shortening equalization for coherent ofdm doubly selective channels,” *Proc. Int. Conf. Acoust. Speech Signal Process*, vol. 4, pp. 361–364, 2006.
- [31] X. Ma, R. J. Baxley, J. Kleider, and G. T. Zhou, “Superimposed training for channel shortening equalization in ofdm,” *Proc. Milcom*, Oct 2006.

- [32] B. Li, S. Zhou, M. Stojanovic, L. Freitag, and P. Willet, “MIMO OFDM over an underwater acoustic channel,” in *in Proc. IEEE Oceans’07 Conference*, (Vancouver, Canada), October 2007.
- [33] B. Li, J. Huang, S. Zhou, K. Ball, M. Stojanovic, L. Freitag, and P. Willet, “Further results on high-rate MIMO-OFDM underwater acoustic communications,” in *in Proc. IEEE Oceans’08 Conference*, (Quebec City, Canada), September 2008.
- [34] T. Kang, H. Song, and W. S. Hodgkiss, “Experimental results of multicarrier communications in shallow water,” in *in Proc. of the 10th European Conference on Underwater Acoustics*, (Istanbul, Turkey), July 2010.
- [35] “Actup v2.2la acoustic toolbox user-interface and post-processor: Installation and user guide.”